# Continental liquid water cloud variability and its parameterization using Atmospheric Radiation Measurement data

Byung-Gon Kim[1]

Atmospheric and Oceanic Sciences Program, Princeton University, Princeton, New Jersey, USA

Stephen A. Klein[2]

Geophysical Fluid Dynamics Laboratory, Princeton University, Princeton, New Jersey, USA

Joel R. Norris

Scripps Institution of Oceanography, University of California, San Diego, La Jolla, California, USA

[1] Liquid water path (LWP) variability at scales ranging from roughly 200 m to 20 km in continental boundary layer clouds is investigated using ground-based remote sensing at the Oklahoma site of the Atmospheric Radiation Measurement (ARM) program. Twelve episodes from the years of 1999 to 2001 are selected corresponding to conditions of overcast, liquid water single-layered cloud. In contrast to previous studies of marine boundary layer clouds, variability in cloud-top height in these clouds is comparable to that of cloud base, and most continental clouds appear to be subadiabatic. In agreement with previous studies of marine boundary layer clouds, variations in LWP are well related to the variations in cloud thickness. LWP variability exhibits significantly negative correlation with the static stability of the inversion near cloud top; larger cloud variability is associated with less stable inversions. A previously developed parameterization of LWP variability is extended to account for the differing conditions of continental clouds. The relationship between fluctuations in LWP and cloud thickness suggests that cloud parameterizations treating variations in LWP at these scales should include the effects of subgrid-scale fluctuations in cloud thickness. One such treatment is proposed within the context of a statistical cloud scheme.

**Citation:** Kim, B.-G., S. A. Klein, and J. R. Norris (2005), Continental liquid water cloud variability and its parameterization using Atmospheric Radiation Measurement data, *J. Geophys. Res.*, *110*, D15S08, doi:10.1029/2004JD005122.

## 1. Introduction

[2] Cloud parameterizations in global atmospheric models have been recognized for decades as a large source of uncertainty in predicting climate change [*Arakawa*, 1975; *Charney*, 1979; *Intergovernmental Panel on Climate Change (IPCC)*, 2001]. Despite some significant progress, problems still remain. For instance, variability in cloud properties at scales smaller than those resolved by large-scale models may cause significant biases because processes such as cloud microphysics and radiation are nonlinear and model calculations do not generally take this into account. Many observational and modeling studies [*Barker et al.*, 1999; *Pincus et al.*, 1999; *Pomroy and Illingworth*, 2000; *Fu et al.*, 2000; *Tiedtke*, 1996] have already shown that correct representation of cloud variability is important for accurate calculation of radiative fluxes for a large variety of cloud situations.

[3] Cloud inhomogeneity in particular reduces the albedo relative to that of a horizontally homogeneous cloud with the same mean optical depth [*Cahalan et al.*, 1994]. However, the information needed to predict cloud variability is generally not available in most large-scale models, although new cloud parameterizations are attempting to predict this variability. In the earliest cloud parameterizations, a simple binary assumption concerning the fractional cloud cover in each grid cell was adapted if any substantial amount of cloud condensate is present. Clearly this assumption of total or zero cloud cover is not appropriate for the horizontal resolution used by global-scale models. A group of schemes subsequently attempted to represent partial cloud cover by relating cloud cover to relative humidity (RH) [*Sellers*, 1976; *Sundqvist*, 1978; *Slingo*, 1980; *Lohmann and Roeckner*, 1996; *Del Genio et al.*, 1996], with cloud cover increasing monotonically from zero at some critical RH according to a specified function. Note that none of these schemes attempted to predict internal cloud inhomogeneity. One way to treat internal cloud inhomogeneity is through statistical schemes, which originated from the works of *Sommeria and Deardorff* [1977] and *Mellor* [1977]. In these schemes, a probability distribution function (PDF) is assumed to represent the subgrid-scale variations of total water (the sum of water

---

[1]Now at Department of Atmospheric Environmental Sciences, Kangnung National University, Gangnung, Gangwondo, Korea.
[2]Now at Atmospheric Science Division, Lawrence Livermore National Laboratory, Livermore, California, USA.

**Table 1.** Summary of Primary Instrumentation and Value-Added Products[a]

| Instrument | Measured Quantities | Comments | Temporal Resolution, s | References |
|---|---|---|---|---|
| Microwave radiometer (MWR) | liquid water path (LWP) | uses microwave brightness temperature; the accuracies are about 20 g m$^{-2}$ for LWP below 200 g m$^{-2}$ and 10% for LWP above 200 g m$^{-2}$, respectively | 20 | *Liljegren* [2000] |
| Active Remotely-Sensed Cloud Locations (ARSCL) | cloud boundaries | Best estimates from MMCR and Ceilometer with resolutions of 45 m and 7.6 m, respectively. | 10 | *Clothiaux et al.* [2000] |
| Balloon-Borne Sounding System (BBSS) | temperature (T), relative humidity (RH), wind speed (WS) | sounding at 6 hour intervals (3 hour interval for intensive observation period) | 10 | www.arm.gov/instruments/static/bbss.stm |

[a]Data sets resulting from assimilation and analysis of data from multiple instruments.

vapor and cloud condensate). This PDF can be used to determine the PDF of cloud condensate from which domain averaged process rates can in turn be calculated.

[4] Indeed, the application of a statistical cloud scheme to the case of a well-mixed boundary layer leads to an analytical expression for the PDF of liquid water path (LWP) that has been compared to observations [*Considine et al.*, 1997] (hereinafter referred to as CCW97). A wide variety of PDFs have been used in these efforts due to difficulties in obtaining generalized and accurate information from observations concerning variability down to small scales. Aircraft and tethered balloon measurements taken for short periods of time usually have undersampling and representativeness problems, and currently available satellite data have difficulties in vertically resolving water vapor and cloud structure. However, ground-based remote sensing has the advantage of continuous operation over long periods that sample an enormous range of conditions, albeit from a fixed point. Well-instrumented sites have integrated data sets available for detailed analysis. Through the efforts of the Atmospheric Radiation Measurement (ARM) program [*Ackerman and Stokes*, 2003], the retrievals of the geometrical boundaries of cloud layers from lidar and radar measurements have been substantially improved. In this study, the rich suite of data from the ARM Southern Great Plain (SGP) site is used to study variability in low-level cloud properties and its relationship to other parameters.

[5] Although many cloud types deserve attention, this study concentrates on liquid water stratus clouds for several reasons. First of all, microwave radiometers can reliably measure LWP, which plays a major role in determining the clouds' radiative impact [*Dong et al.*, 2002; *Kim et al.*, 2003]. Secondly, low stratus clouds have a major impact on the shortwave radiative budget of the planet [*Hartmann*, 1993]. Thirdly, the relative simplicity of the boundary layer cloud permits one to test ideas of how clouds should vary and thus has been a major focus of previous studies of cloud variability [e.g., CCW97] (see also *Wood and Taylor* [2001], hereinafter referred to as WT01). Finally, unlike marine stratus clouds, continental stratus clouds have been relatively overlooked in spite of their strong influence on local weather, their radiative impacts on the diurnal cycle, and their interactions with air pollution [*Sassen et al.*, 1999; *Zhu et al.*, 2001].

[6] The outline of the paper is as follows. Section 2 presents the data and method used in this study. Section 3 examines the variability of continental cloud properties, including cloud base height, top height, thickness, and LWP, and focuses on the relationship between cloud LWP variability and cloud thickness. Meteorological influences on LWP variability are also examined by contrasting the LWP variability between cases. Section 4 modifies the prior parameterizations (CCW97 and WT01) of LWP variability in the light of the observations presented herein and section 5 discusses a method to represent cloud inhomogeneity in climate models. Section 6 presents the conclusion for this study.

## 2. Data and Method

[7] The data for this study are from the ARM archive (http://www.archive.arm.gov). The most favorable cloud type for our purposes is an overcast, liquid water cloud without interference from higher-level ice clouds. Higher-level ice clouds were excluded due to their greater complexity. Since the selected cases have cloud temperatures above 273 K most of the time, the clouds can be regarded as liquid phase only. For simplification, this study considers only single layered clouds and not overlapped or multilayered clouds. Suitable conditions are carefully selected by subjective examination of time series of retrieved cloud layers at SGP during 1999–2001.

[8] Table 1 summarizes the primary instruments used in this study. Cloud boundaries are retrieved every 10 s from the Active Remotely Sensed Cloud Locations (ARSCL) value-added product, which combines data from active remote sensors, mainly the Millimeter Wave Cloud Radar (MMCR), micropulse lidar, and ceilometer [*Clothiaux et al.*, 2000]. For the present analysis, the radar data and some available ceilometer data are mostly used. The height resolutions of radar, and ceilometer are 45 m, and 7.6 m, respectively. Although the radar generally provides very accurate estimates of cloud base height, its sensitivity to large cloud droplets such as drizzle droplets means that the radar underestimates the true cloud base in the presence of drizzle. For this reason, the cloud base is preferably retrieved from the ceilometer, which is not so sensitive to large droplets. Accordingly, cloud geometric thickness is defined as the difference between the radar-derived cloud-top height and the laser ceilometer-derived cloud base

height. However, the ceilometer data are not always available, so the statistics for cloud base and cloud thickness from both instruments will typically be shown. The radar also tends to give a higher cloud base in case of no drizzle because of the low sensitivity to very small droplets at the cloud base. Unfortunately, ceilometer data is available for only half of the selected cases. Nevertheless, the discussion will be limited mainly to the statistics of the data retrieved from the ceilometer.

[9] Time series measurements of column-integrated amounts of water vapor and liquid water are provided from the Microwave Radiometer (MWR), a sensitive microwave receiver. Vertical liquid water path at SGP is measured every 20 s by a zenith-viewing Radiometerics WVR-1100 MWR operating at frequencies of 23.8 and 31.4 GHz [*Liljegren*, 2000]. Liquid water in the atmosphere emits in a continuum dominating the 31.4 GHz channel, whereas water vapor dominates the 23.8 GHz channel. The root mean square accuracies of the LWP retrievals are about 20 g m$^{-2}$ for LWP below 200 g m$^{-2}$ and 10% for cloud LWP above 200 g m$^{-2}$, respectively [*Liljegren et al.*, 2001]. A new retrieval of LWP recently created by *Liljegren et al.* [2001] was not available in time for this study. Although a newer algorithm for LWP retrieval (2001) is being adopted by the ARM community [*Liljegren et al.*, 2001], prior experience with boundary layer clouds observed at the ARM SGP [*Kim et al.*, 2003] indicated rather good agreement between the two approaches with similar temporal variation.

[10] Atmospheric vertical structure is obtained by the Balloon-Borne Sounding System (BBSS), which provides vertical profiles of the thermodynamic state of the atmosphere and wind speed and direction. Pressure, temperature, relative humidity, wind speed, and wind direction are obtained every 10 s during a free-balloon ascent. Balloons are usually launched 4 times a day but 8 times a day during Intensive Observation Periods. However, many of the selected periods lack vertical soundings.

[11] Because the raw data includes large-scale mean temporal variability in addition to advected spatial variability, the subject of this study, time series for each parameter such as cloud boundaries, thickness, and LWP were detrended by subtracting 30-min running averages. As described in Appendix A, pixel-level satellite data was used to compare the magnitude of temporal change in spatially averaged optical thickness with the spatial standard deviation of optical thickness. The results suggested that advection of spatial variability would contribute at least 75% of the variance in optical thickness seen over a single point during a 30 min time interval. Although longer averaging intervals could be used in some cases, a 30-min interval guarantees that temporal changes in the cloud field have little impact on the following analyses. For an average horizontal wind speed of 10 m s$^{-1}$, the spatial scales examined in this study are limited to less than around 20 km, which is a fairly typical grid scale of numerical weather prediction model and, as a result, the variability in this study is also representative of the variability that needs to be parameterized in such mesoscale models. Because of the temporal resolution of the data ($\sim$20 s), the smallest scales examined are about 200 m. Thus the variability studied herein corresponds to spatial scales varying from

the larger turbulent scales to the smaller mesoscale. The radiation smoothing scale in clouds is of order 200–400 m so that variability in cloud liquid water at spatial scales less than 200 m can be neglected in terms of the cloud-radiation parameterization [*Davis et al.*, 1997]. Note that it might be a more crucial omission to exclude the variability at the opposite end of the spectrum (i.e., variability on spatial scales greater than $\sim$20 km) because climate models have resolutions much bigger than $\sim$20 km.

[12] The statistics examined in this study include the standard deviation, skewness, and dispersion of the detrended time series of variables such as the cloud base, cloud top, cloud thickness, and LWP. For any such variable $x$, the standard deviation ($\sigma$) for each 30-min interval p is defined with respect to the running mean as

$$\sigma_{x,p} = \left[ \frac{\sum_i^N \left( x_{o,i} - x_{m,i} - \delta_x \right)^2}{N_p} \right]_p^{1/2} = \left[ \frac{\sum_i^N \left( x'_{o,i} - x'_{m,i} \right)^2}{N_p} \right]_p^{1/2} \quad (1)$$

where $x'_{o,i} = x_{o,i} - \overline{x_{o,i}}$, $x'_{m,i} = x_{m,i} - \overline{x_{m,i}}$, $\delta_x = \sum_i^N (x_{o,i} - x_{m,i})/N_p$ and $x_{m,i}$ is the 30-min running average of the original data $x_{o,i}$. $\bar{x}$ is the time average over each 30 min and $N_p$ is the number of data points available for each 30 min interval $p$. Equation (1) is very similar to an equation of conventional standard deviation except for $\delta_x$, which is the average of difference between original data ($x_{o,i}$) and the 30-min running average ($x_{m,i}$).

[13] The dispersion ($D$) and skewness ($S$) are obtained as follows;

$$D_{x,p} = \frac{\sigma_{x,p}}{\overline{x_{o,i}}} \quad (2)$$

$$S_{x,p} = \frac{\sum_i^N \left( x_{o,i} - x_{m,i} - \delta_x \right)^3 / N_p}{\sigma_{x,p}^3} = \frac{\sum_i^N \left( x'_{o,i} - x'_{m,i} \right)^3 / N_p}{\sigma_{x,p}^3} \quad (3)$$

## 3. Cloud Variability

### 3.1. Overview

[14] There are 12 analysis days during the years 1999–2001 that meet the selection criteria of overcast, single layered, and liquid phase clouds for continuous periods of three hours or more. Table 2 summarizes statistics related to the mean and the variability of cloud base height, top height, thickness, and LWP. The mean LWP varies from 70 to 480 g m$^{-2}$, and the mean cloud base and top heights are also highly variable with thicknesses ranging from 250 to 2500 m. The standard deviations ($\sigma_b$ and $\sigma_t$) of cloud base and top heights range from 15 to 227 m and 45 to 106 m, and $\sigma_t$ is generally equal to or larger than $\sigma_b$. Accordingly, $\sigma_h$ is also variable, ranging from 50 to 267 m. The dispersion of cloud thickness is typically less than 0.2, consistent with the findings of *Smith and Del Genio* [2002]. Likewise, the variance in LWP varies strongly with case with values of $\sigma_{lwp}$ varying from 9 to 120 g m$^{-2}$). Although the standard deviation of LWP is in general larger for larger mean LWPs, the dispersion of LWP is not constant and ranges from 0.1 to 0.36. No systematic patterns

**Table 2.** Summary of the Mean of Base Height $C_b$, Top Height $C_t$, Thickness $h$, and LWP of Clouds and Standard Deviation $\sigma$, Skewness $S$, and Dispersion $D$ of the Anomalies $C_b'$, $C_t'$, $h'$, and LWP'[a]

| Case | Period, UTC | Mean | | | | Standard Deviation | | | | Dispersion | | Skewness | | | |
|---|---|---|---|---|---|---|---|---|---|---|---|---|---|---|---|
| | | $C_b$, m | $C_t$, m | $h$, m | LWP, g m$^{-2}$ | $\sigma_b$, m | $\sigma_t$, m | $\sigma_h$, m | $\sigma_{lwp}$, g m$^{-2}$ | $D_h$ | $D_{lwp}$ | $S_h$ | $S_{LWP}$ | $\gamma/r(lwp,h)$ | Thermodynamic/Drizzle |
| | | | | | | | | | *1999* | | | | | | |
| 2/1 | 0800–1800 | *590* | | *357* | | *33.9* | | *54.0* | | *0.15* | | *0.28* | | 0.68/(0.62) | mixed to stable/drizzle |
| | | 315 | 947 | 632 | 131 | 27.5 | 45.1 | 53.7 | 14.7 | 0.08 | 0.11 | 0.24 | 0.37 | | |
| 3/23 | 1200–2400 | *698* | | *257* | | *53.6* | | *74.0* | | *0.28* | | *−0.64* | | 0.55/(0.62) | mixed/drizzle |
| | | 371 | 955 | 584 | 96 | 97.7 | 53.2 | 106.5 | 18.0 | 0.18 | 0.19 | −0.45 | 0.52 | | |
| 5/17 | 1500–1900 | 323 | 1097 | 773 | 229 | 58.9 | 95.4 | 100.6 | 59.9 | 0.13 | 0.26 | −0.51 | 0.90 | | mixed/NA |
| 10/4 | 0400–0800 | 495 | 851 | 356 | 72 | 17.5 | 56.4 | 58.6 | 8.8 | 0.16 | 0.12 | 0.72 | −0.07 | | mixed/NA |
| | | | | | | | | | *2000* | | | | | | |
| 2/18 | 0900–1500 | *327* | | *734* | | *45.8* | | *75.3* | | *0.10* | | *0.13* | | 0.94/(0.77) | mixed/drizzle |
| | | | 1061 | | 155 | | 60.0 | | 32.9 | | 0.21 | | 0.59 | | |
| 3/15 | 1200–1700 | *329* | | *493* | | *16.1* | | *50.6* | | *0.10* | | *0.86* | | 0.98/(0.79) | stable to mixed/drizzle |
| | | 181 | 822 | 640 | 147 | 15.3 | 46.6 | 51.1 | 19.6 | 0.08 | 0.13 | −0.53 | 0.47 | | |
| 3/17 | 1900–2300 | *219* | | *1570* | | *28.6* | | *54.8* | | *0.03* | | *0.58* | | 3.49/(0.50) | two adjacent mixed layer/drizzle |
| | | 149 | 1789 | 1640 | 474 | 14.0 | 45.4 | 49.9 | 47.5 | 0.03 | 0.10 | 0.82 | 0.21 | | |
| 3/19 | 1100–1600 | *520* | | *458* | | *50.7* | | *71.9* | | *71.9* | | *−0.60* | | 1.15/(0.74) | mixed/no drizzle |
| | | 415 | 977 | 563 | 114 | 45.6 | 50.1 | 69.7 | 26.1 | 0.12 | 0.23 | −0.98 | 0.45 | | |
| 10/6 | 1800–2100 | 2596 | 3456 | 860 | 103 | 75.8 | 79.3 | 120.3 | 24.0 | 0.14 | 0.23 | −0.77 | 0.25 | | midlevel stable/NA |
| | | | | | | | | | *2001* | | | | | | |
| 4/16 | 1200–2000 | 1747 | 4267 | 2520 | 331 | 226.7 | 105.8 | 266.7 | 118.9 | 0.10 | 0.36 | 0.19 | 1.05 | | mixed/NA |
| 5/31 | 1200–1900 | 660 | 1455 | 794 | 188 | 40.8 | 63.0 | 73.6 | 37.2 | 0.09 | 0.20 | −0.09 | 0.40 | | mixed/NA |
| 9/24 | 0800–1600 | 1094 | 1382 | 288 | 100 | 24.7 | 46.3 | 51.1 | 12.2 | 0.18 | 0.12 | 0.39 | 0.08 | | mixed/NA |

[a]Also given are the correlation coefficient r between LWP and $h$, and $\gamma$, the exponent of a power law regression obtained by fitting the data to the equation LWP = $\alpha h^{\gamma}$. Italic values are obtained/calculated from the ceilometer. Refer to Figure 6. Brief indications of the thermodynamic state and presence of drizzle for each case are provided in the final column. NA: not available.

occur in cloud thickness skewness whose absolute values are generally less than 1.0 indicative of relatively weak skewness. For LWP, most skewness values are positive with a slight tendency for larger LWP dispersion accompanying larger skewness. This is expected for a quantity that is bounded by zero on the low side. Nonetheless it would not be a great error to assume that most LWP PDFs are nearly symmetric. Symmetric PDFs appear to be characteristic of overcast cloud fields (CCW97 and WT01), though CCW97 showed the PDFs of effective optical thickness.

[15] The available vertical soundings of equivalent potential temperature ($\theta_e$) indicate that most cloud cases generally occur within well-mixed boundary layers. Two exceptions are episodes on 6 October 2000 and 15 April 2001 when the cloud layer existed above the mixed layer. Most clouds exist just below an inversion that caps the mixed layer. The presence of drizzle can be determined by a radar reported cloud base lower than that determined from the ceilometer. Drizzle was found to occur in five out of the six cases that this could be tested.

### 3.2. Episode Analysis

[16] Figures 1 and 2 exhibit time series of base height, top height, thickness, and LWP of clouds on 1 February 1999 and 19 March 2000, respectively. The first day corresponds to a case of low LWP variability ($\sigma_{lwp}$ = 15 g m$^{-2}$) and drizzle case, and the latter is one of relatively higher LWP variability ($\sigma_{lwp}$ = 26 g m$^{-2}$) and nondrizzle case. Besides, these episodes are preferable because they are also coincident with the intensive observation period, and thus the vertical soundings at 3-hourly interval are available. In addition, as both days have the ceilometer data as well as the radar data, the drizzle can be identified.

[17] On 1 February of 1999 (Figure 1), the cloud base reported by the ceilometer varies from approximately 500 to 800 m, whereas the cloud top varies from 800 to 1200 m. As expected, cloud thickness variation is strongly associated with LWP variation. LWP increases sharply around 1500 UTC (local time is 6.5 hours earlier than UTC) together with the deepening of cloud thickness following sunrise. In contrast, LWP and cloud thickness remain almost steady during the night. Following 1500 UTC, the cloud gradually thins. Vertical soundings of potential temperature and mixing ratio of water vapor indicate the cloud layer is well-mixed at 0829 UTC and 1130 UTC but notably weakly stable at 1428 UTC and 1728 UTC (Figure 3a). After sunrise, the inversion is less strong and less sharp. The cloud boundaries (black thick lines in Figure 3a) match the vertical soundings of temperature and water vapor especially at night such that vertically well-mixed structures of equivalent potential temperature occur and mixing ratios of water vapor nearly equal the saturation mixing ratio within the clouds. One exception is the sounding at 1428 UTC when the cloud base is located about 300 m above the height assumed from the sounding. During the period, the sounding wind profiles (not shown) indicate that the low level stratus is advected northeastward with a gradual increase of wind speed during the case from $\sim$5–8 to $\sim$12–15 m s$^{-1}$.

[18] Temporal variations of the PDF of detrended anomalies in cloud base, cloud top, cloud thickness, and LWP ($C_b'$, $C_t'$, $h'$ and LWP') are also shown in Figures 1 and 2. The PDF of anomalies for each 30-min interval is displayed along the vertical axis, and each PDF is based on the ARSCL and MWR measurements with bin sizes of $C_b$, $C_t$, and $h$ of 50 m and LWP of 20 g m$^{-2}$. The PDFs for
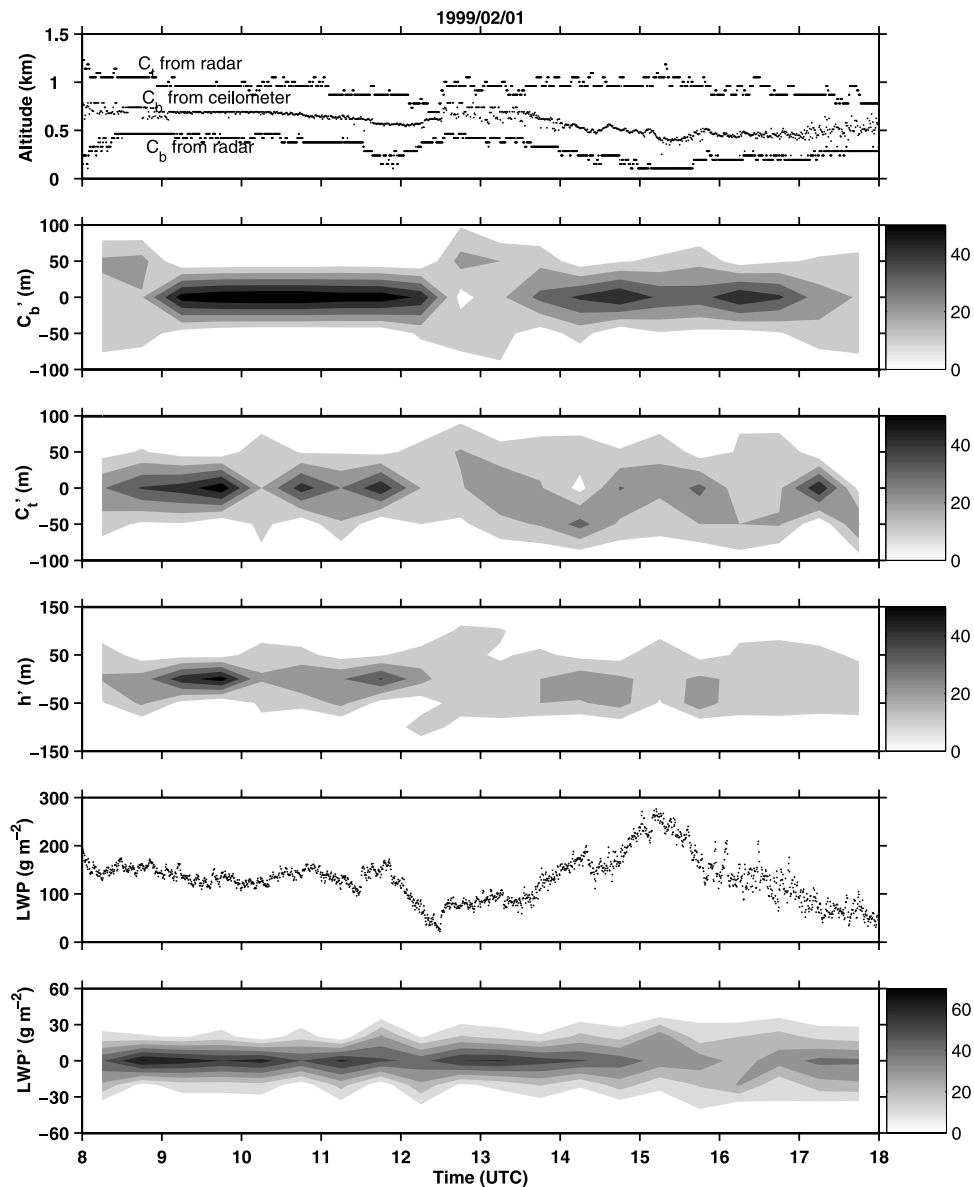
**Figure 1.** Time series of cloud boundaries (base height $C_b$, top height $C_t$), cloud thickness $h$, and LWP on 1 February 1999, also with PDFs of their anomalies ($C_b'$, $C_t'$, $h'$, and LWP'). For each 30-min. interval the PDF of anomalies is shown along the vertical axis and the PDFs for various times are shown one after another along the horizontal axis. See color version of this figure at back of this issue.

various times are presented one after another along the horizontal axis. Cloud-top variability is almost comparable to cloud base variability for timescales less than 30 min, and fluctuations in cloud base are uncorrelated with those of cloud top (r = 0.1), a general feature of these cases. The cloud base PDF is narrow at night but wider during the day. This pattern also occurs in cloud top, cloud thickness, and LWP PDFs and may be associated with the change in the potential temperature gradient, as seen in Figure 3a. A strong nighttime inversion weakens after the sunrise; the inversion strength measured by the difference of potential temperature from the inversion base to cloud-top height divided by the height difference changes from ∼0.05–0.06 K m$^{-1}$ at night to 0.03 K m$^{-1}$ during the day.

[19]  Similar to the 1 February 1999 case, unbroken cloud exists from 1100 to 1600 UTC on 19 March 2000 within the

well-mixed layer with cloud top (1000 m) just above the inversion base (Figure 2). As seen in the vertical soundings of 1130 UTC and 1430 UTC (Figure 3b), the cloud boundaries are consistently well-matched with those assumed from the vertical soundings of equivalent potential temperature and mixing ratio of water vapor within the clouds, similar to Figure 3a. In fact, there is even better agreement between mixing ratio and saturation mixing ratio of water vapor in the cloud layer. On this day the cloud is thicker with the mean thickness of 500 m. In contrast to the previous case, the PDFs of $h'$ and LWP' are broader, and the difference of potential temperature from the inversion base to cloud-top height divided by the height difference is only ∼0.02– 0.03 K m$^{-1}$, relatively weaker stability than on 1 February 1999. The relationship of cloud variability to the measured soundings will be discussed further in section 3.4.
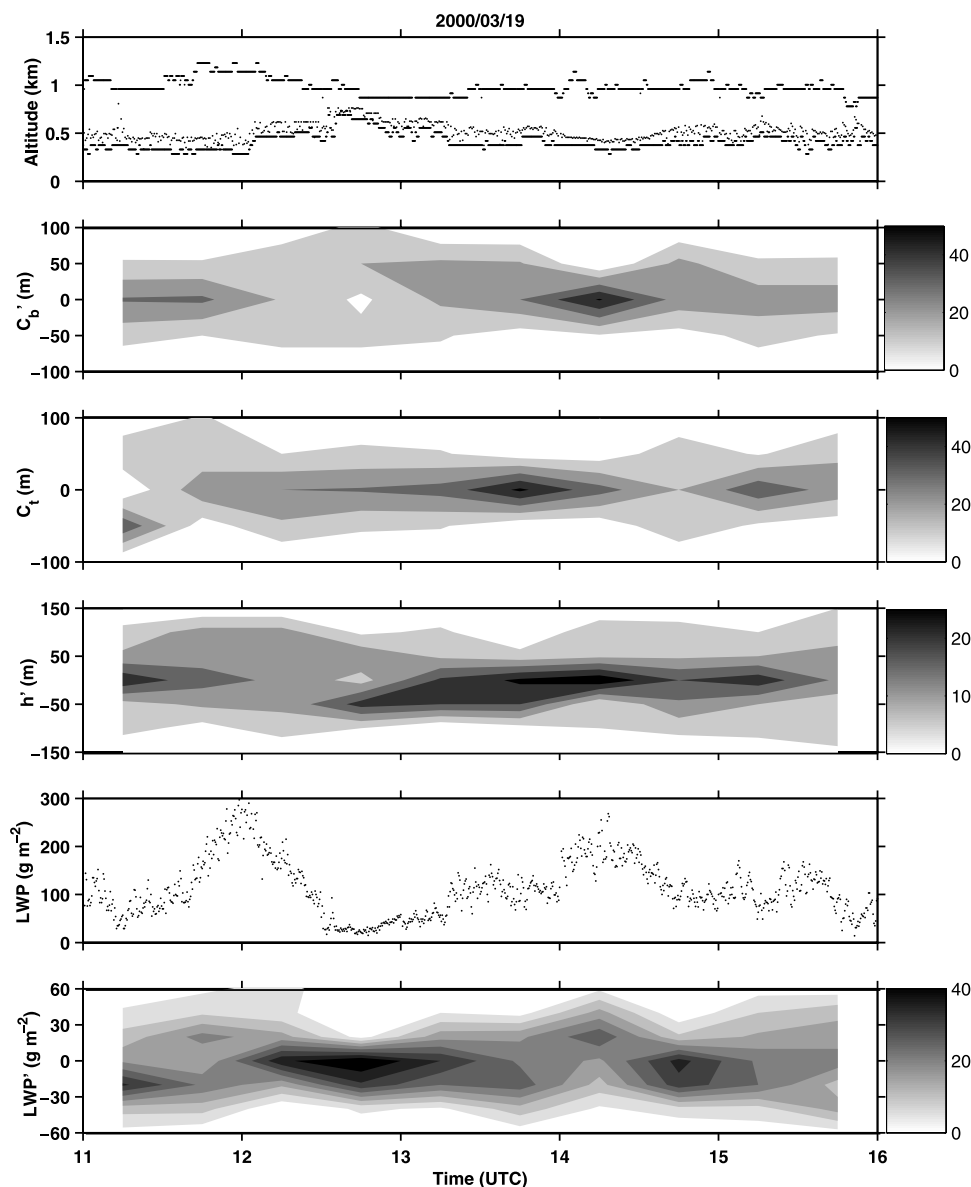
**Figure 2.** The same as in Figure 1 but for 19 March 2000. See color version of this figure at back of this issue.

[20] In Figure 1, drizzle can be identified from the ~200–300 m discrepancy in cloud base identified by the ceilometer and the radar. Cloud base boundaries from the radar are observed to be consistently lower than those from the ceilometer. Because the radar return is proportional to sixth power of cloud drop size, and the ceilometer return is proportional to the square of cloud drop size, the radar is more sensitive to the large drops that occur beneath cloud base. However, little drizzle appears to be observed in the 19 March case (Figure 2). Cloud base boundaries from the radar are almost adjacent to those from the ceilometer within twice of the radar resolution (50 m). As previously noted, drizzle is common in these overcast clouds (Table 2); 5 cases of the 6 cases indicate the presence of drizzle when both ceilometer and radar observations are available. In addition, the cloud reflectivity has been examined in order to confirm the presence of drizzle. Figure 4 shows time-height plot of MMCR reflectivity at SGP for the same

periods as in Figures 1 and 2. The cloud boundaries assumed from reflectivity larger than −40 dBZ agree well with those of top panels of Figures 1 and 2. *Frisch et al.* [1995] indicated the cloud reflectivity in excess of −15 dBz is indicative of drizzle. The reflectivities of 1 February 1999 are consistently larger than −15 dBZ from 1130 to 1600 UTC with the high reflectivities extending downward, indicative of drizzle occurring, whereas those of 19 March 2000 are less than −20 dBZ during the whole period. Furthermore, the drizzle pattern is quite different from *Bretherton et al.* [2004, Figure 7] (a heavy drizzle period of reflectivity up to 10 dBZ) in the study of marine boundary layer cloud, which showed significant mesoscale variability in drizzle patches within even a short timescale (2 and half hours period). The PDFs of $C_b'$, $C_t'$, $h'$, and $LWP'$ are shown in Figure 5 for the entire period of each day (1 February 1999 and 19 March 2000). The calculation is done in the same manner as in Figures 1 and 2 but for the
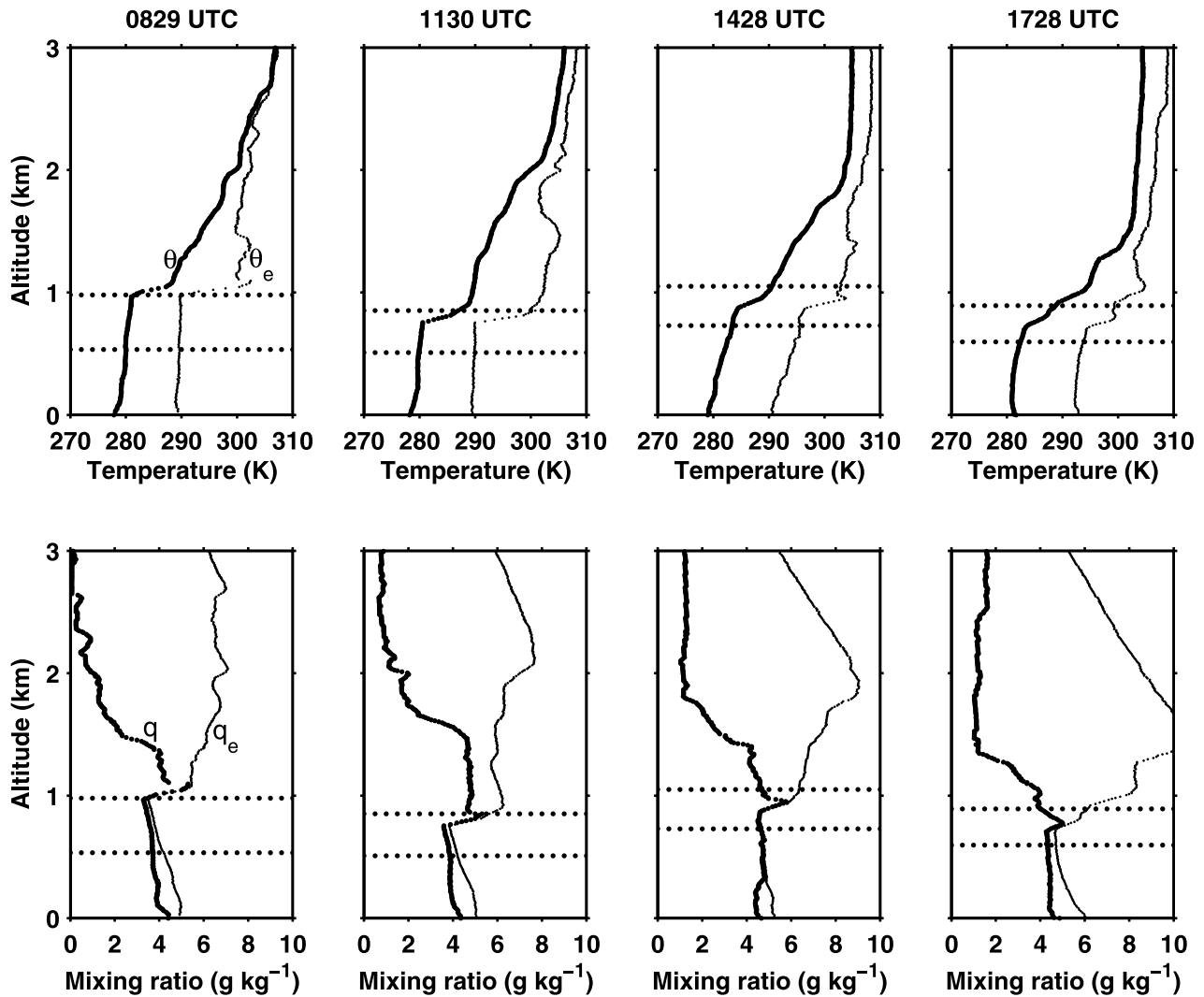
**Figure 3a.** Vertical profiles of (top row) potential temperature θ and equivalent potential temperature θ$_e$ and (bottom row) mixing ratio q, and saturation mixing ratio q$_e$ in the lower panel on 1 February 1999 and 19 March 2000. The black dotted line indicates the cloud boundaries.

whole overcast period. In general, the PDFs of $C'_b$, $C'_t$, $h'$, and LWP$'$ are quasi-symmetric distribution with a small positive skewness. The PDFs of $C'_b$ and $C'_t$ distributions on both days are generally similar to each other, whereas the PDFs of $h'$ and LWP$'$ on 19 March 2000 are broader compared to those on 1 February 1999, which is consistent with Figures 1 and 2.

### 3.3. Relationship of LWP to Cloud Thickness

[21] Stratocumulus clouds exhibit adiabatic liquid water content [*Slingo et al.*, 1982; *Albrecht et al.*, 1990; *Gerber et al.*, 1994; *Brenguier et al.*, 2000] and sometimes subadiabatic liquid water content [*Austin et al.*, 1995; *Nicholls and Leighton*, 1986; *Miller et al.*, 1998]. This section examines the degree of adiabacity through the relationship between LWP and cloud thickness. In order to quantify adiabacity, the adiabatic LWP (LWP$_{ad}$) can be defined on the basis of LWC linearly increasing with height above the cloud base [*Albrecht et al.*, 1990]:

$$LWP_{ad} = \Gamma_{ad}h^2/2, \qquad (4)$$

where

$$\Gamma_{ad} = \frac{(\varepsilon + q_s)q_s l_v}{R_d T^2}\Gamma_w \qquad (5)$$

is the adiabatic change of LWC with height, $\varepsilon = 0.622$, $q_s$ is the saturation mixing ratio of water vapor, $h$ is the cloud thickness, $l_v$ is the latent heat of vaporization, R$_d$ is the specific gas constant for dry air, and $\Gamma_w$ is the moist adiabatic lapse rate. $\Gamma_{ad}$ is calculated using the mean temperature $T$ and pressure $P$ at the level of the cloud from the available soundings.

[22] Using equation (4), the degree of adiabacity (DOA) can be estimated from the ratio of observed LWP versus adiabatic LWP (Table 3). DOA is obtained using the cloud base from the ceilometer. The value of the DOA ranges from 0.20 to 1.53; the cloud is superadiabatic if the DOA is larger than 1, and the cloud is subadiabatic if the DOA is less than 1. Aside from the nearly adiabatic case (1999/2/1) and superadiabatic case (1999/3/23), subadiabatic clouds are diagnosed from the values of DOA. Most continental
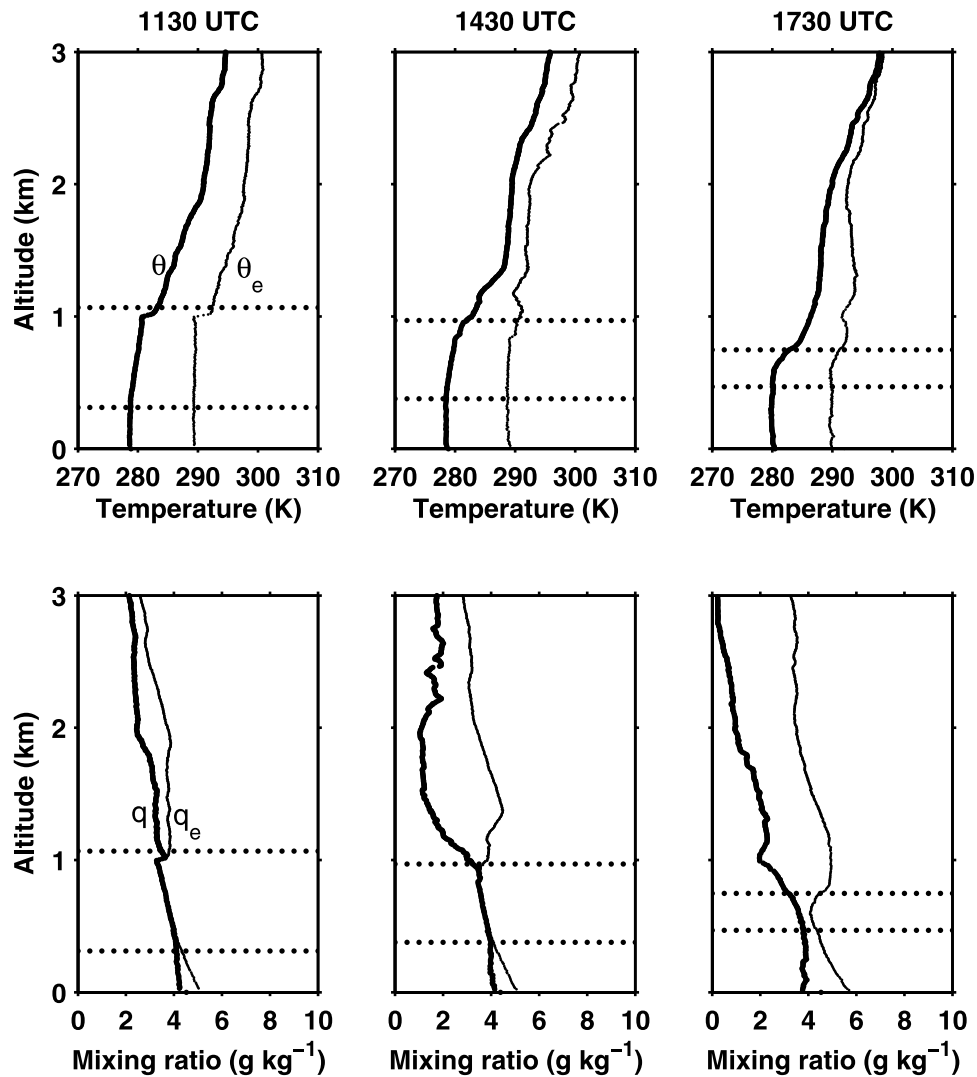
**Figure 3b.**   Same as in Figure 3a except for 19 March 2000.

clouds observed in this study therefore appear to be subadiabatic probably as a result of the frequent occurrence of drizzle, a nonadiabatic process. Observations of apparently "superadiabatic" clouds are possible when there is cumulus rising beneath a strong inversion as shown in the work of *Miller et al.* [1998]. Unfortunately it is hard to associate the 23 March case with this hypothesis because the lack of soundings prevented identification of conditional instability needed for cumulus under stratocumulus. Figure 6 displays scatterplots of LWP versus cloud thickness for days with ceilometer data. Note that the data have been fitted to the equation LWP = $\alpha h^{\gamma}$, and the x and y axes have decimal logarithm scales. Cloud LWP exhibits a roughly linear dependence on cloud thickness but with slopes that vary from day to day ($\sim$0.5–3.5). The significant correlation (r > 0.5) demonstrates that LWP variability is closely related to cloud thickness variability. It is interesting to note that the episode average of each slope appears to be around 1.2 although the slope for an adiabatic cloud is 2. When the linear axes are used rather than the logarithmic scales, the correlation between LWP and cloud thickness shows also good correlation (r = 0.63–0.80) except for 17 March 2000 (r = 0.49). There are at least 2 possible reasons for the near-

linear relationship of LWP against cloud thickness. First, the thicker the cloud the more likely drizzle occurs. This would preferentially lower LWP at the high end of the cloud thickness distribution. Second, sampling error may lower the slope of the logarithmic correlation. A Monte Carlo test consisting of adding random observational error to synthetic time series of LWP and cloud thickness, which obeyed a quadratic relationship, lowered the logarithmically determined slope from 2 to 1.5. The random errors assigned LWP and cloud thickness were 20 g m$^{-2}$ and 90 m consistent with Table 1. Meanwhile, the slopes for drizzle days are generally lower than that for nondrizzle day except for 17 March 2000. The steepest slope (3.5) of 17 March 2000 is thought to be associated with distinctive vertical structure on this day, when two adjacent mixed layers occurred over the depth of the cloud. The quantitative analysis of drizzle effect on adiabacity is worthy of the future study.

[23]  A simple scaling analysis for variability of detrended LWP (LWP′) now follows. Figure 7 plots the standard deviation of LWP′ against the mean value for 30-min intervals from all of the 12 whole episodes. Least squares linear regressions performed on the data in Figure 7 show a
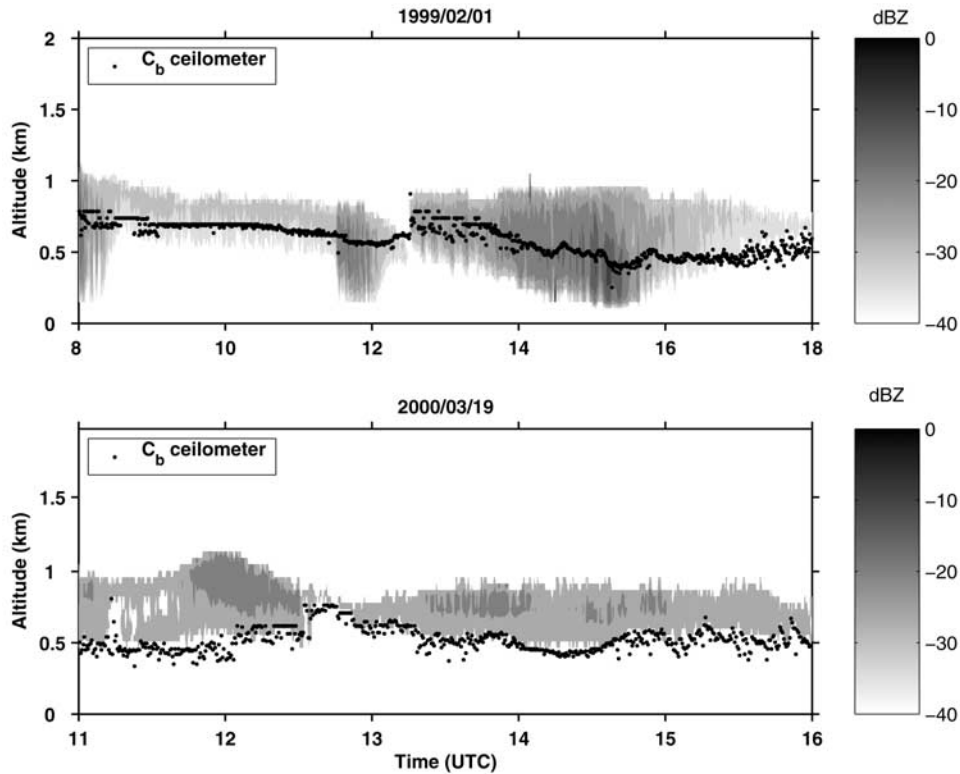
**Figure 4.** Time-height plot of MMCR reflectivity (dBZ from −40 to 0) at SGP on 1 February 1999 and 19 March 2000. Black dots indicate the cloud base from the ceilometer. See color version of this figure at back of this issue.

linear correlation of $\sigma_{lwp}$ with the mean quantity, indicating the spatial variation of LWP is sensitive to an increase in its mean value. This result is similar to the linear relationship between mean LWP and $\sigma_{lwp}$ from satellite retrievals of marine boundary clouds in the work of *Wielicki and Parker* [1994]. The level of correlation is statistically significant (r = 0.7), but the relationship has much scatter.

[24] In order to understand the association of LWP variability with that of cloud thickness variability, the standard deviation ($\sigma$), dispersion (*D*) and skewness (*S*) of LWP$'$ and $h'$ are examined within 30-min intervals (Figure 8). For this figure, $h'$ is calculated using only ceilometer data. The standard deviation of LWP is poorly correlated with $\sigma_h$. A large part of the substantial variability in the scatterplot is due to the data of 17 March 2000. Removing this particular case from the scatterplot improves the correlation from 0.12 to 0.32, but it is still not significant. The weak correlation implies that the LWP variability for timescale less than 30 min is not significantly associated with the cloud thickness variability. In addition to this simple scaling approach, the scaling analysis of equation (6) in WT01 has been also examined but this did not improve the correlation. The plots of *S* and *D* between LWP and *h* exhibit better correlation; greater skewness in *h* is associated with greater skewness in LWP and great dispersion in *h* is associated with greater dispersion in LWP.

## 3.4. Meteorological Influences

[25] In addition to simple scaling relationships for variability of LWP and cloud thickness, it is worthwhile examining the role of larger-scale meteorological processes. This section investigates the relationship of cloud variability to the thermodynamic structure and wind fields measured by the available soundings. The relationship of cloud variability to the Brünt-Väisälä frequency $N^2$ (= $(g/\theta)\partial\theta/\partial z$) and the vertical wind shear $W$ (= $\partial|\vec{u}|/\partial z$) in the cloud layer are of particular interest and scatterplots are shown in Figure 9. $N^2$ and $W$ are calculated using the difference in $\theta$ and $|\vec{u}|$ between cloud base and cloud top.

[26] Table 4 lists the results of similar analyses applied to $N^2$ and $W$ calculated over different layers such as from the inversion base to cloud top, or from the cloud base to inversion base. Note that the base of the inversion is mostly located between cloud top and cloud base (i.e., the sounding in Figure 3). The differing heights to cloud top and inversion base may be due to error in radiosonde or radar height measurements and/or the spatial displacement of the radiosonde when it passes through cloud top from the fixed ground base station at which the radar is located. Furthermore, the visible cloud is only one part of the cloud-generating environment, which is mostly larger than the real cloud, which may also explain why the cloud top does not exactly match up with the inversion base from the sounding. Conclusions are tentative because the number of available comparisons is 14 for the relationship of LWP variability to $N^2$ and $W$ and, due to the unreliability of $C_b$ from the radar, only 11 for the relationship of cloud thickness variability to $N^2$ and $W$. The standard deviations of LWP and $h$ are those from the nearest 30-min period containing the sounding.
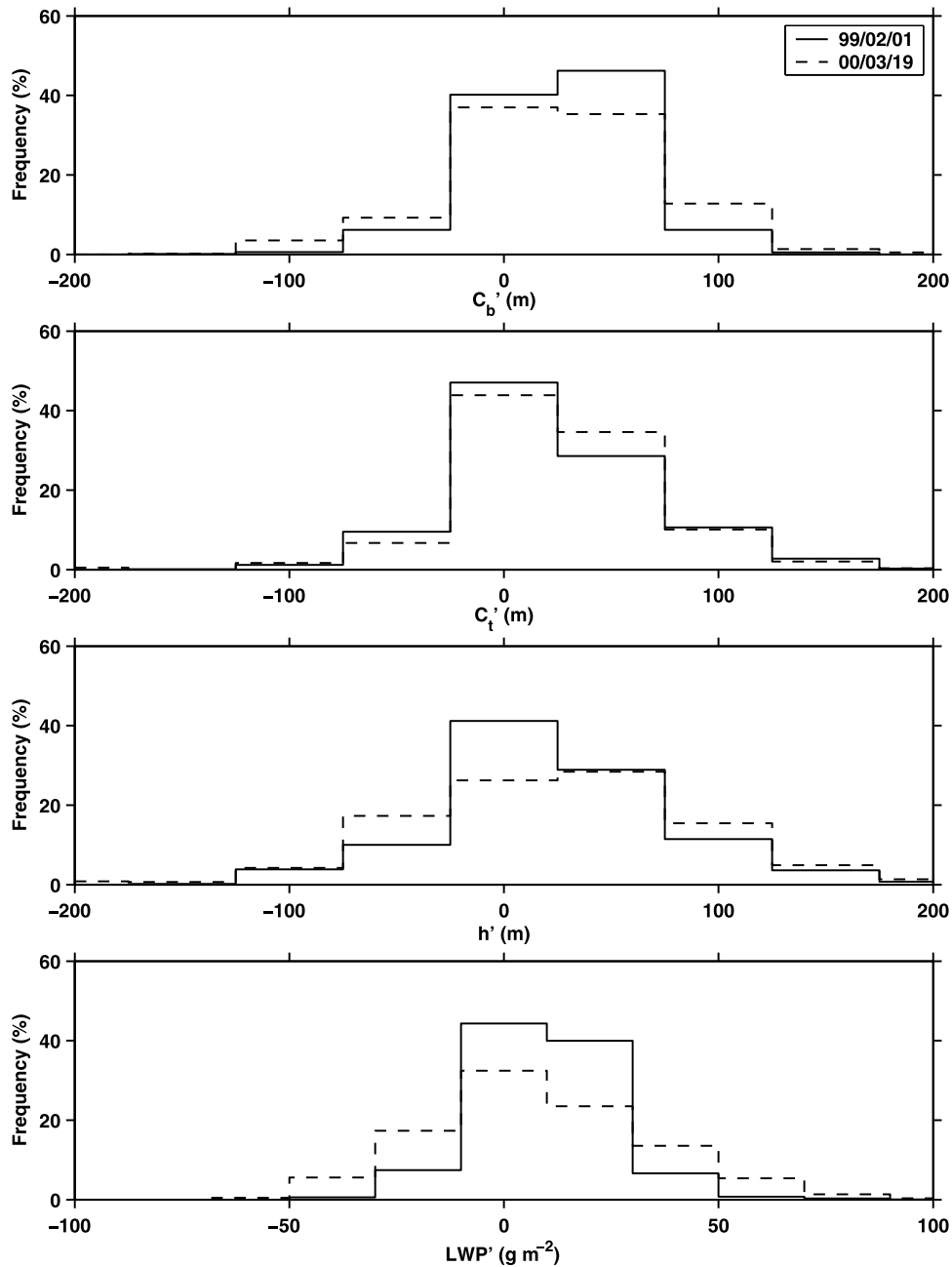
**Figure 5.** Histograms of the anomalies ($C_b'$, $C_t'$, $h'$, and LWP') of base height, top height, thickness and LWP of clouds on 1 February 1999 and 19 March 2000. The calculation is done in the same manner as in Figures 1 and 2 but for the period from 0800 to 1800 UTC and from 1100 to 1600 UTC, respectively.

[27] Variability in cloud LWP exhibits significant negative correlation (r = −0.79) with $N^2$ for the layer from cloud base to cloud top; stronger static stability is associated with decreased cloud variability. The association of stronger stability with lower LWP variability suggests that the suppression of turbulence in the inversion by the vertical static stability reduces cloud variability. Similar comparisons using the equivalent potential temperature in the calculation of $N^2$ resulted in negative correlation (r = −0.67) between the moist $N^2$ and $\sigma_{lwp}$.

[28] However, this hypothesis is contradicted by the negative correlation between LWP and $W$; the higher

vertical wind shear, the lower spatial variability in LWP. This compensation causes the Richardson number $Ri$, a variable widely used to indicate the potential for mixing (defined as $N^2$ divided by $W^2$), to exhibit a relatively weak positive correlation with the $\sigma_{lwp}$. Variability in cloud thickness is also negatively correlated with the static stability (r = −0.54), suggesting that the stability of the inversion limits the extent to which turbulent eddies penetrate the inversion. If the same approach is applied to the layer of the inversion base to cloud top, it is interesting to note that the association of static stability with that of the inversion layer is implied by the even larger correlation (r = −0.85)

**Table 3.** Degree of Adiabacity DOA, Adiabatic Change of LWC With Height $\Gamma_{ad}$, and Correlation Coefficient r for the Analysis Period[a]

| | 1999 | | 2000 | | | |
| --- | --- | --- | --- | --- | --- | --- |
| | 1 Feb. | 23 March | 18 Feb. | 15 March | 17 March | 19 March |
| DOA | 1.04 | 1.53 | 0.31 | 0.49 | 0.20 | 0.62 |
| $\Gamma_{ad}$,[b] g kg$^{-1}$ km$^{-1}$ | 1.77 | 1.67 | 1.78 | 2.34 | 1.89 | 1.59 |
| r[c] | 0.65 | 0.68 | 0.74 | 0.79 | 0.46 | 0.70 |

[a]DOA = $\overline{LWP_{ob}}$ / $\overline{LWP_{ad}}$, $\overline{LWP_{ob}}$ is the mean of observed LWP, and $\overline{LWP_{ad}}$ is the mean of adiabatic LWP calculated from equation (4) using cloud base from the ceilometer.

[b]$\Gamma_{ad} = \frac{(\varepsilon + q_s)q_s l_v}{R_d T^2}\Gamma_w$, $\varepsilon = 0.622$, $l_v$ is the latent heat of vaporization, $R_d$ is the specific gas constant for dry air, and $\Gamma_w$ is the moist adiabatic lapse rate.

[c]Here r is the correlation coefficient of observed LWP with adiabatic LWP and significant to 99% confidence level.

between the variability in LWP and $N^2$ as measured from inversion base to cloud top. The relationships between skewness and dispersion of LWP and $h$ to $N^2$ and wind shear are generally not significant (Table 4). One exception is the significant negative correlation between LWP skewness and $N^2$, for which we do not have an explanation.

## 4. Parameterization of LWP Variability

### 4.1. Model Update

[29] While liquid water path variability may differ between cases for many reasons such as the variable nature of entrainment, static stability and mechanical turbulence, the conceptual model of CCW97 and WT01 could however account for the essential features of liquid water path variability. WT01 and CCW97 related cloud thickness variability to thermodynamic variability of subcloud layer using the assumption that cloud base fluctuations are the dominant contributor to cloud thickness variability. This assumption may be reasonable for the marine stratus clouds examined in their study since the strong subsidence inversion strongly damps motions in the inversion layer. In this study an updated version of the CCW97 and WT01 models is proposed on the basis of the differing characteristics of continental boundary layer cloud.

[30] All motions in the model of CCW97 are assumed to follow a moist adiabatic such that the LWC of a given parcel will be approximately linear with height above the cloud base, with the slope determined by the moist adiabatic. As in equation (5), the vertical gradient of *LWC* $d(LWC)/dz$ is defined to be $\Gamma_{ad}$, and *LWC* can be easily integrated to give LWP proportional to the square of cloud thickness. Because LWP is uniquely related to cloud thickness, it is possible to derive a PDF of LWP by association of the PDF of cloud thickness with the PDF of LWP (CCW97)

$$P(LWP)d(LWP) = P(h)dh, \qquad (6)$$

where $P(h)$ is the PDF of the cloud thickness, and $P(LWP)$ is the PDF of LWP.

[31] The current analysis of continental boundary clouds with ground-based remote sensing documents cloud phenomena that differ from the assumptions made by CCW97 and WT01. First, the variation of the cloud-top height is

comparable to and in most cases greater than that of cloud base height. Second, continental clouds are frequently not adiabatic. In this case, one might assume that, similar to equation (4), the LWP is uniquely related to the square of cloud thickness but with a different slope $\Gamma'$ obtained by the assuming a nonadiabatic cloud with cloud thickness h is given by

$$LWP = \Gamma' h^2 / 2 \qquad (7)$$

where $\Gamma'$ might represent the rate of LWC increase with height within the cloud and is obtained from the slope of the plot of cloud LWP versus the square of cloud thickness.

[32] With the assumption of cloud thickness being normally distributed with the standard deviation $\sigma_h$, the PDF of LWP can be given as in CCW97 and WT01

$$CPDF = \frac{1}{\sqrt{4\pi\Gamma'\sigma_h^2 LWP}} \exp\left\{ -\frac{\left\{ LWP^{1/2} - \left(\overline{LWP} - \Gamma'\sigma_h^2/2\right)^{1/2} \right\}^2}{\Gamma'\sigma_h^2} \right\} \qquad (8)$$

where $\sigma_h$ is the standard deviation of cloud thickness and $\overline{LWP}$ is the mean of LWP. The modifications to the original model are the use of a different slope $\Gamma'$ and the replacement of the standard deviation of cloud base with that of cloud thickness.

[33] The regression illustrated in Figure 6 indicates the relationship between LWP and cloud thickness is closer to linear than quadratic. Thus the second empirical probability distribution function (EPDF) for LWP is proposed using a linear relationship between cloud thickness and LWP

$$LWP = \Lambda' h \qquad (9)$$

where $\Lambda'$ is the slope of plot of cloud LWP versus cloud thickness and is also equal to the mean LWC in the cloud with the assumption of $\Lambda'$ being constant.

[34] Similarly, if cloud thickness is normally distributed, then LWP PDF is

$$EPDF = \frac{1}{\sqrt{2\pi}\sigma_h\Lambda'} \exp\left\{ -\frac{\left(LWP/\Lambda' - \bar{h}\right)^2}{2\sigma_h^2} \right\} \qquad (10)$$

where $\bar{h}$ is the mean cloud thickness $h$. After all, if cloud thickness and its standard deviation can be provided by the radar cloud boundary data, all of the input parameters required by the PDFs are determined from the observations.

### 4.2. Comparisons of PDFs

[35] Comparisons of estimated PDFs of LWP with the observed PDF are presented in Figure 10 for the six episodes with ceilometer-retrieved cloud bases. The model PDFs are calculated from equations (8) and (10) using the mean LWP from the observations along with $\sigma_h$ determined after first linearly detrending the data. The observed PDF of detrended LWP is based on the MWR measurement, and displayed with the offset of the mean LWP. Note first that both of the proposed PDFs are nearly similar to each other.
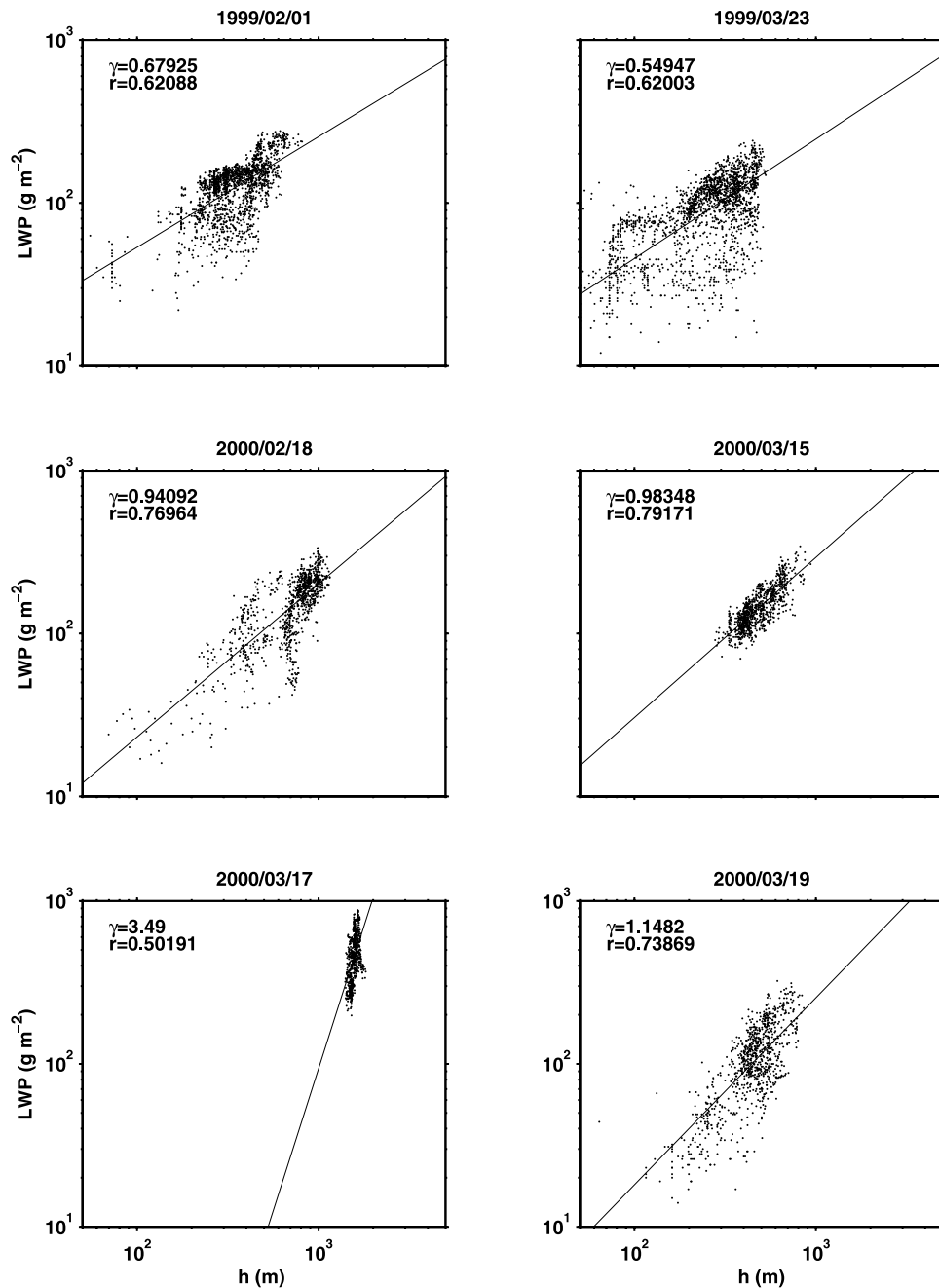
**Figure 6.** Scatterplots of LWP versus cloud thickness for the analysis period on different days. The data have been fitted to the equation LWP = $\alpha h^{\gamma}$ and the x and y axes have decimal logarithm scales. The plot is limited to six cases with ceilometer data.

The fact that the proposed PDFs agree well with the observed one means that scaling the standard deviation of LWP by that of the cloud thickness is effective for explaining the spread in LWP. The model predicts a quasi-normal distribution to liquid water, consistent with CCW97 for overcast conditions. Although the linear dependence of LWP on cloud thickness is supported by very few five cases (Figure 6) and an empirical result, the empirical PDFs of this study yield results similar to the PDFs from CCW97 and WT01.

[36] The estimated EPDF and CPDF of LWP appear to be wider than the observed PDF on 1 February 1999. The standard deviation of LWP is relatively smaller than that of cloud thickness, and the ratio of $\sigma_{lwp}$ to $\sigma_h$ is 0.27 (Table 2). This situation also occurs on 23 March 1999. It is obvious that the width of distributions is dependent upon the ratio of $\sigma_{lwp}$ to $\sigma_h$, and episodes with lower ratios ($\sim$0.2–0.3) have estimated PDFs, which are broader than the observed PDFs. Note that cases with lower ratios coincide with lower LWP variability ($\sigma_{lwp}$ = 15–18 g m$^{-2}$).

[37] On 18 February 2000, $\sigma_{lwp}$ is relatively higher (33 g m$^{-2}$), and the EPDF and CPDF of LWP consequently exhibit narrower histograms in contrast to low LWP variability. There is a poor correspondence for the PDF com-
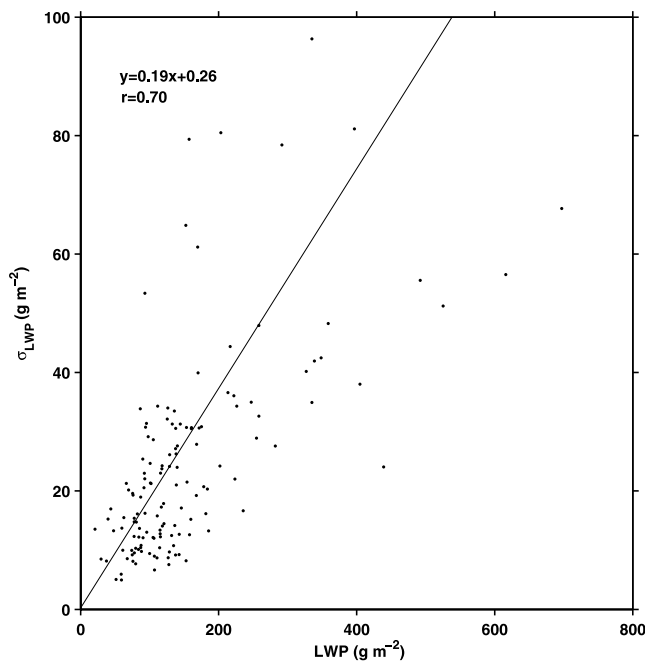
**Figure 7.** Scatterplots of standard deviation σ of the detrended LWP versus the mean quantity for 30-min intervals of the 12 whole episodes. Solid line denotes the regression line for both variables.

parisons on 17 March 2000 when the correlation of $\sigma_{lwp}$ with $\sigma_h$ is weak (Figure 8). This is probably associated with the vertically decoupled structure of two adjacent mixed layers, which is different from the other vertical profiles. The occurrence of cloudiness within two adjacent mixed-layer structures seems to be not applicable to CCW97.

## 5. Discussion on Representing Cloud Inhomogeneity

[38] The results of the previous section indicate that scaling the width of the LWP distribution with that of cloud thickness is reasonable. In applying these results to climate models, the question arises as to how one would predict variability in cloud thickness. Considering that the clouds documented in this paper have cloud thicknesses with a mean and standard deviation of 500 m and 60 m, respectively, climate models would not resolve fluctuations in cloud thickness directly since they have vertical resolutions greater than 100 m, even in the boundary layer. How then can climate models parameterize these fluctuations? Might it be best to use a simple scaling relationship as illustrated in Figure 8 and dispense with more detailed prediction of the subgrid-scale fluctuations in cloud properties and its dependencies on atmospheric state? For these cases this might be so, but assuming that one wants to represent these fluctuations and their dependencies, a method for diagnosing these fluctuations within the context of a statistical cloud scheme with a prognostic equation for the variance of water within a grid box is outlined in this section.

[39] As pointed out by CCW97, their assumption of a Gaussian distribution of cloud bases is equivalent to assuming a Gaussian distribution of total water fluctuations

relative to saturation (essentially relative humidity) within a well-mixed boundary layer. If so, it is reasonable to assume that these fluctuations would be related to the nature of the turbulence in the boundary layer. WT01 proposed that the fluctuations in cloud base could be related to fluctuations in lifting condensation levels that can be predicted from the turbulent scaling theories.

[40] The observations presented in this paper require significant modifications to this model. While it is straightforward to relax the assumption of a well-mixed boundary layer, the more challenging fact to deal with is that cloud thickness fluctuations are in large part manifestations of fluctuations of cloud-top height as well as those of cloud
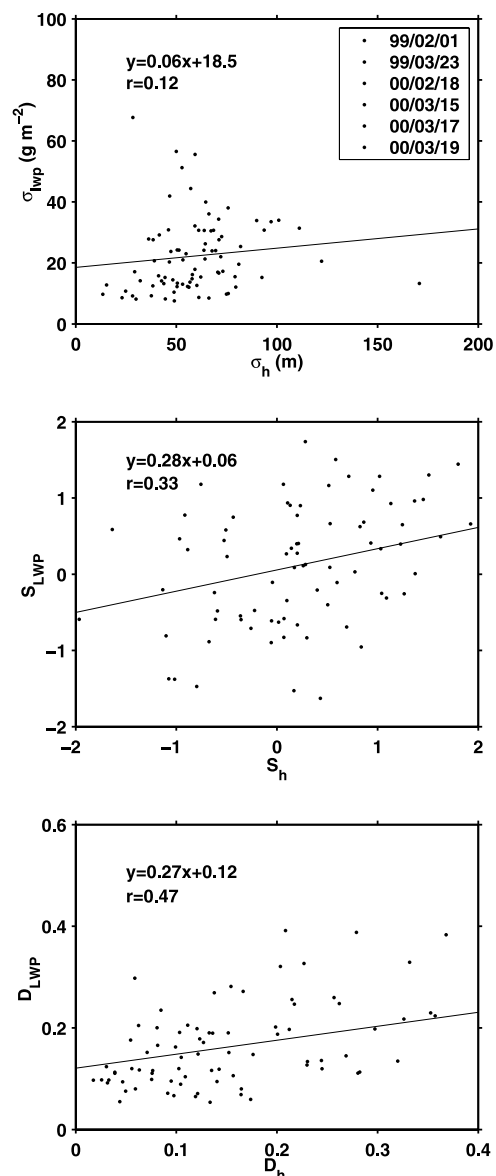


**Figure 8.** Scatterplots of standard deviation σ, skewness S, and dispersion D of the detrended LWP versus those of detrended cloud thickness for 30-min intervals. Solid line denotes the regression line for both variables. These plots are limited to six cases with ceilometer data. See color version of this figure at back of this issue.
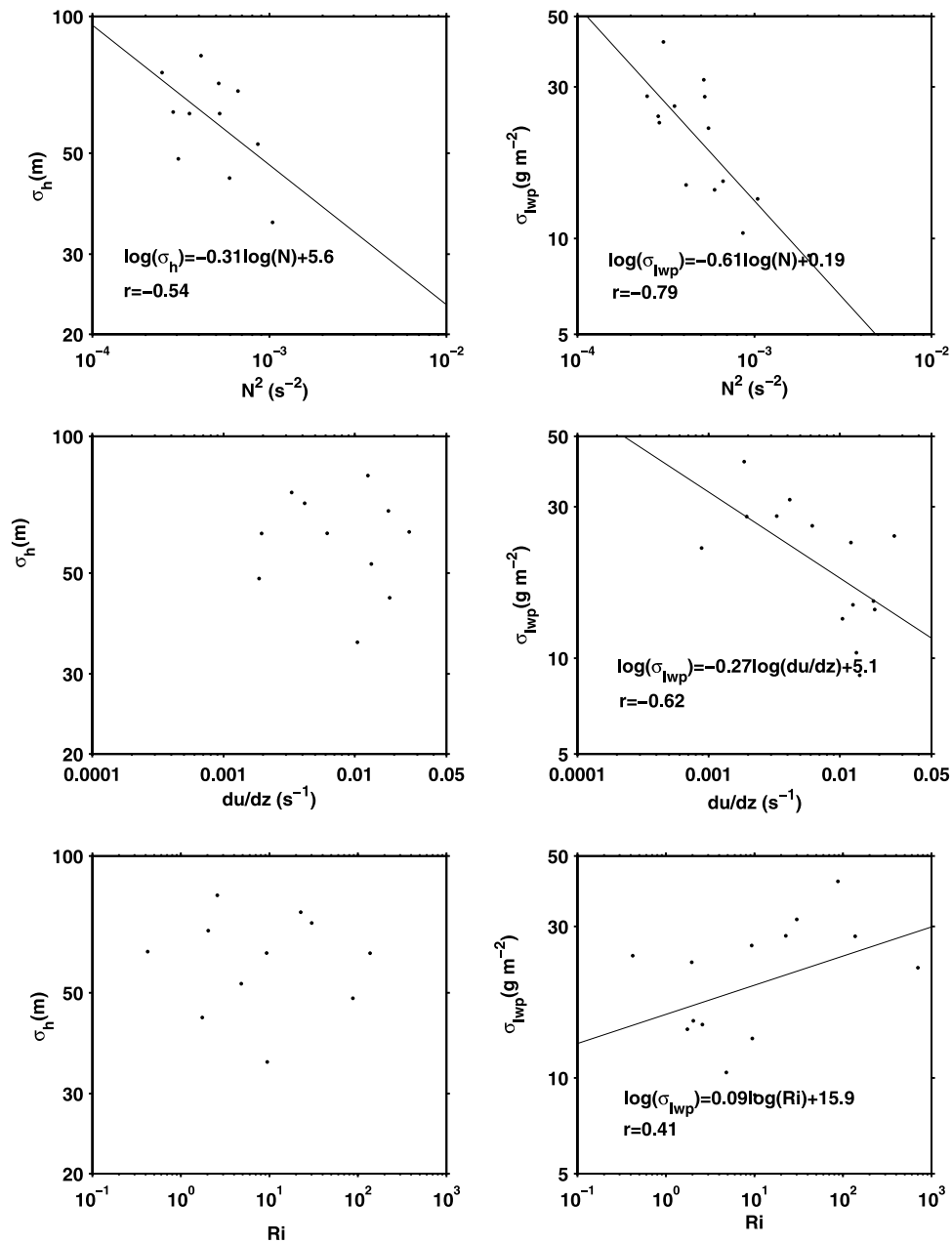
**Figure 9.** Relationships of standard deviations of cloud thickness ($\sigma_h$) and LWP ($\sigma_{lwp}$) to the Brünt-Väisälä frequency $N^2$ ($= (g/\theta)\partial\theta/\partial z$) and vertical wind shear $W$ ($= \partial|\vec{u}|/\partial z$) in the cloud layer. $N^2$ and $W$ are obtained from the available soundings. The number of available comparisons is 14 for the relationship of LWP variability to $N^2$ and $W$ and, owing to the reliability of $C_b$ from the radar, only 11 for the relationship of cloud thickness variability to $N^2$, and $W$.

base height. Evidence presented here suggests that these fluctuations may also be predictable in that greater cloud-top height variability is related to weaker inversions atop the boundary layer. This finding for continental boundary layer clouds is consistent with the study of *Smith and Del Genio* [2001], who found that the dispersion of cloud thickness of cirrus clouds was negatively correlated with the static stability over the depth of the cloud.

[41] What is then needed is a systematic way to relate cloud variability to meteorological conditions. *Tompkins* [2002] proposed a statistical cloud scheme for climate

models in which fluctuations in total water specific humidity were predicted with a prognostic equation for the variance of total water. Under the rigors of a budget equation for total water variance, the competing effects of turbulence within the boundary layer and turbulence in the inversion layer on variability in total water would be weighted appropriately.

[42] Within the statistical cloud scheme approach, one can also treat the issue of subgrid-scale cloud thickness and its fluctuations. The most straightforward interpretation of the statistical cloud scheme approach is that the parameter-

**Table 4.** Correlation of the Variability in LWP with the Brünt-Väisälä Frequency $N^2$, and Vertical Wind Shear $W$ in the Different Layer, Such as From Cloud Base $C_b$ to Cloud-Top $C_t$, From $C_b$ to Inversion Base $Z_i$, and From $Z_i$ to $C_t$[a]

| Layer | Correlation | $N^2$ | $W$ | $Ri$ | Correlation | $N^2$ | $W$ | $Ri$ |
|---|---|---|---|---|---|---|---|---|
| $C_b$ to $C_t$ | $\sigma_{lwp}$ | −0.79 | −0.62 | 0.45 | $\sigma_h$ | −0.54 | −0.10 | −0.03 |
| $C_b$ to $Z_i$ | $\sigma_{lwp}$ | −0.21 | −0.52 | 0.48 | $\sigma_h$ | −0.43 | −0.07 | 0.32 |
| $Z_i$ to $C_t$ | $\sigma_{lwp}$ | −0.85 | −0.63 | 0.44 | $\sigma_h$ | −0.26 | −0.16 | 0.11 |
| $C_b$ to $C_t$ | $D_{lwp}$ | −0.34 | −0.32 | 0.19 | $D_h$ | 0.30 | 0.13 | −0.06 |
| $C_b$ to $Z_i$ | $D_{lwp}$ | 0.16 | −0.17 | 0.27 | $D_h$ | 0.06 | 0.36 | −0.34 |
| $Z_i$ to $C_t$ | $D_{lwp}$ | −0.30 | −0.49 | 0.44 | $D_h$ | 0.48 | 0.10 | −0.01 |
| $C_b$ to $C_t$ | $S_{lwp}$ | −0.53 | 0.17 | −0.50 | $S_h$ | 0.14 | 0.46 | −0.45 |
| $C_b$ to $Z_i$ | $S_{lwp}$ | −0.33 | 0.02 | −0.18 | $S_h$ | −0.48 | 0.15 | −0.44 |
| $Z_i$ to $C_t$ | $S_{lwp}$ | −0.26 | 0.13 | −0.20 | $S_h$ | 0.07 | 0.49 | −0.50 |

[a]Note that the correlation coefficient is obtained in the decimal logarithmic scales of standard deviations of LWP and $h$, and those of $N^2$ and $W$, and linear correlation is applied for the dispersion and skewness.

ized total water PDF represents only horizontal fluctuations, as opposed to both horizontal and vertical fluctuations. This is the assumption used in the Reynolds averaging for the total water variance budget equation and is the only plausible assumption that will permit convergence as the vertical resolution increases. If one assumes that the vertical variation of the horizontally averaged temperature and total water within a single grid box are known, and if one assumes that there are no vertical variations in the horizontal fluctuations parameterized by the total water PDF, then one knows completely the three dimensional structure of the clouds (although of course, not their relative placement in the horizontal). Drawing a random sample from the PDF, one has complete information on the vertical profile of cloud liquid and water vapor, and knowledge of any cloud bases or tops within this grid box. These random samples could then be used to compute radiation fluxes [*Pincus et al.*, 2003], thus eliminating the radiation bias due to assuming horizontally homogeneous clouds in radiation calculations of climate models.

[43] Are these assumptions used to diagnose subgrid-scale variations in cloud tops and bases reasonable? The first assumption is that one knows the subgrid vertical structure to the mean total water and temperature. Climate models already make assumptions about this structure, for purposes of vertical advection calculations among other things. One would just apply an assumption from another part of the climate model to determine the cloud. The second assumption is that the horizontal fluctuations in total water have no vertical dependence within a single grid box. This is reasonable, at least in part, because cloud radar observations indicate maximum cloud overlap is a better assumption as the physical separation distance decreases [*Hogan and Illingworth*, 2000].

## 6. Conclusions

[44] Ground-based remote sensing of cloud boundaries and LWP has been used to determine cloud variability and structure during 1999−2001 over the Southern Great Plains. Twelve overcast episodes are selected that meet requirements of low-level nonprecipitating, liquid water single-layered cloud.

[45] Several interesting conclusions have arisen. First of all, variability in cloud-top height is almost comparable to that of cloud base, which is not the case for previously studied marine boundary layer clouds. Moreover, most continental clouds appear to be subadiabatic. Another distinct feature is that the cloud thickness variations are closely associated with the LWP variations, and less stable inversions tend to increase the variability of cloud LWP. A previously developed parameterization of LWP is updated to account for the differing conditions observed for continental clouds, and good agreement between the model and the observations is exhibited. Lastly, an approach for diagnosing the subgrid-scale fluctuation in cloud properties is discussed within the context of a statistical cloud scheme.

[46] From this empirical study, LWP variability is closely related to cloud thickness variability. To accurately represent this variability in global climate models will require a parameterization for subgrid-scale variations in cloud thickness. An extension of the present study would be analysis of partly cloudy episodes, which are expected to have cloud property distributions that are more skewed.

## Appendix A

[47] The use of a single-point time series to study spatial variability assumes the processes controlling cloud properties are stationary. Since this is true only over limited timescales, it is critical to determine what these timescales are. Removal of a running mean with the length of this timescale then ensures that advected spatial variability is the dominant contributor to variability of the single-point time series. This study determined the appropriate timescale for the single-point time series analysis by examining half-hourly pixel-level cloud optical thickness data processed from daytime GOES-8 radiances by *Minnis et al.* [2002]. These data were available for only three of the episodes listed in Table 2. Each multihour episode had extensive low-level stratiform cloud cover within a $1° \times 1°$ grid box centered on the SGP site that contained approximately 640 pixels of 4 km size. A very small number of pixels with higher-level cloudiness were discarded in order to focus on liquid water clouds. Table A1 lists mean cloud fraction, mean cloud optical thickness, and the spatial standard deviation of cloud optical thickness over the grid box for each half hour. One measure of the relative importance of temporal and spatial variability is the ratio of change in mean optical thickness over an hour divided by the spatial standard deviation. These ratios provide guidance for choosing the optimal running mean timescale to remove from single-point time series.

[48] Typical values of this ratio range from 0.35 to 0.6, but substantial variability occurs, even from one hour to another (Table A1). This indicates that there is no single timescale applicable to all situations. As a worst case scenario (1715 UTC on 31 May 2001), the change in the mean optical thickness over an hour is equal to the spatial standard deviation. This is equivalent to half the spatial standard deviation over 30 min, or 25% of the variance. The median change in mean optical thickness over 30 min is one quarter of the spatial standard deviation, or about 6% of the variance. Removal of a 30-min running mean from a single-point LWP time series eliminates almost all of the nonsta-
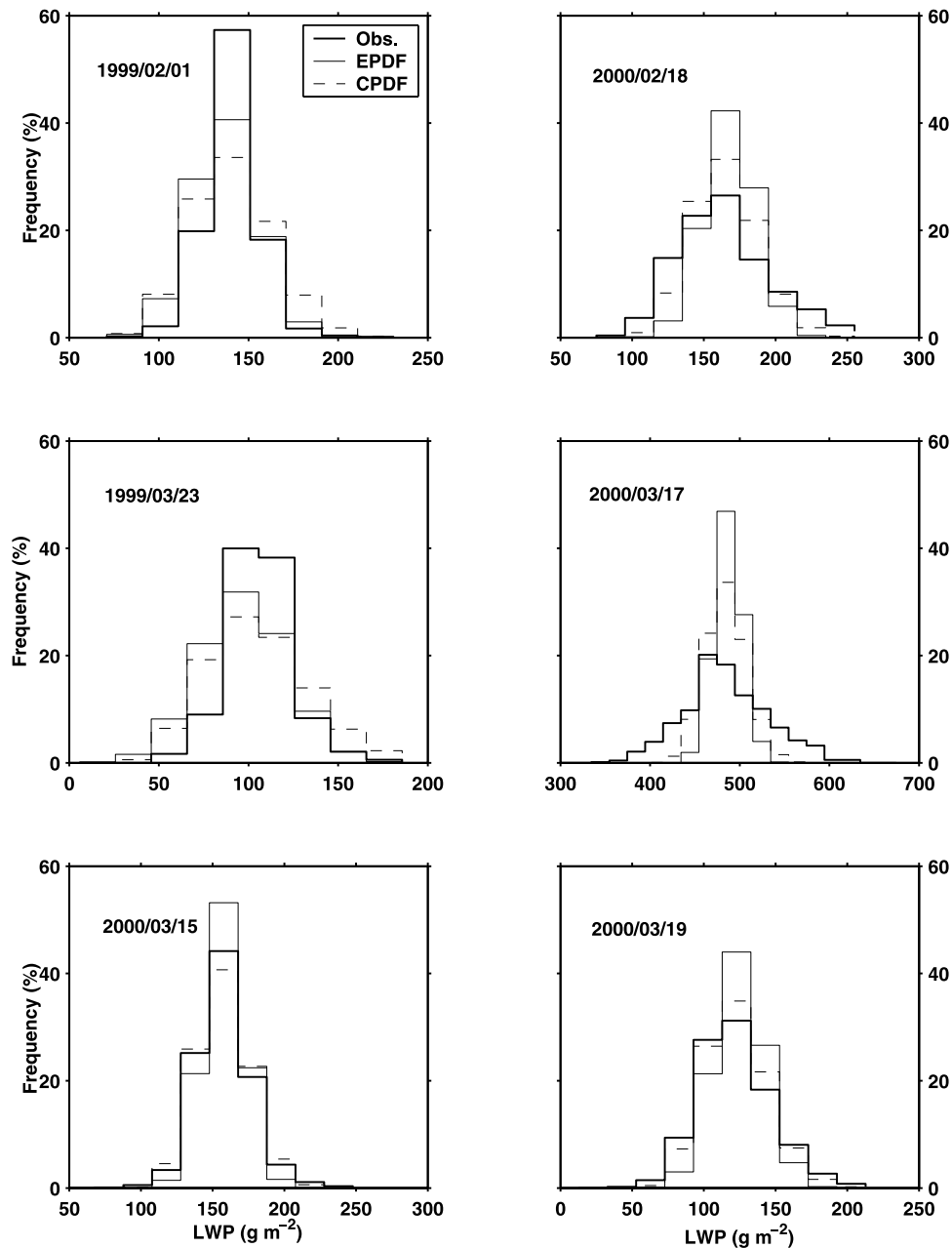
**Figure 10.** Comparison of the estimated PDFs of LWP to the observed one (thick line) for six episodes with ceilometer data. The model PDFs are calculated from equations (8) and (10) using the mean LWP from the observations along with $\sigma_h$ determined after first linearly detrending the data. The observed PDF of detrended LWP is based on the MWR measurement, and displayed with the offset of the mean LWP.

tionary change in cloud optical thickness. A 30-min time-scale corresponds to a distance scale of 18 km for an advection speed of 10 m s$^{-1}$, so a large portion of mesoscale spatial variability is unfortunately eliminated as well. It is difficult to distinguish between temporal change and mesoscale spatial variability in a single-point time series.

[49] The importance of mesoscale variability was assessed by calculating the fraction of variance contributed by different spatial scales. Pixel cloud optical thickness was averaged in grid squares with sizes of 0.125°, 0.25°, and

0.5°, corresponding to approximately 12 km, 25 km, and 50 km. The variance at spatial scales below 0.125° was determined by subtracting the variance of 0.125° values from the variance of pixel values. Similarly, the variance at spatial scales between 0.125° and 0.25° was determined by subtracting the variance of 0.25° values from the variance of 0.125° values, and so on. The variance at spatial scales between 0.5° and 1° was assigned to be the variance of 0.5° values. Table A1 shows the fraction of variance at different scales every half hour. The majority of the variance occurs at scales less than ∼12 km and/or more than ∼50 km, with

**Table A1.** Satellite Cloud Statistics for the Region 36–37°N, 97–98°W[a]

| Time, UTC | Cloud Fraction | $\bar{\tau}$ | $\sigma$ | $\frac{\bar{\tau}_{n+1}-\bar{\tau}_{n-1}}{\sigma_n}$ | Fraction of Variance at Different Spatial Scales | | | |
|---|---|---|---|---|---|---|---|---|
| | | | | | Pixel–0.125° | 0.125°–0.25° | 0.25°–0.5° | 0.5°–1° |
| *15 March 2000* | | | | | | | | |
| 1515 | 1.00 | 26.7 | 10.2 | −0.31 | 0.23 | 0.10 | 0.20 | 0.47 |
| 1545 | 0.96 | 25.6 | 11.9 | −0.45 | 0.17 | 0.12 | 0.20 | 0.51 |
| 1615 | 0.89 | 21.4 | 11.9 | −0.33 | 0.15 | 0.07 | 0.11 | 0.68 |
| 1645 | 0.77 | 21.7 | 12.6 | −0.69 | 0.15 | 0.12 | 0.20 | 0.53 |
| *19 March 2000* | | | | | | | | |
| 1445 | 1.00 | 24.3 | 17.9 | −0.35 | 0.33 | 0.10 | 0.15 | 0.42 |
| 1515 | 0.99 | 20.8 | 14.9 | −0.32 | 0.35 | 0.09 | 0.18 | 0.38 |
| 1545 | 0.97 | 19.5 | 13.5 | −0.23 | 0.26 | 0.08 | 0.13 | 0.53 |
| 1615 | 0.89 | 17.7 | 11.9 | −0.41 | 0.30 | 0.08 | 0.19 | 0.44 |
| 1645 | 0.89 | 14.7 | 9.9 | −0.71 | 0.34 | 0.07 | 0.20 | 0.39 |
| 1715 | 0.73 | 10.6 | 6.9 | −0.85 | 0.41 | 0.11 | 0.13 | 0.36 |
| *31 May 2001* | | | | | | | | |
| 1545 | 1.00 | 39.3 | 14.6 | 0.46 | 0.39 | 0.22 | 0.26 | 0.14 |
| 1615 | 1.00 | 41.4 | 12.4 | −0.13 | 0.48 | 0.24 | 0.12 | 0.16 |
| 1645 | 1.00 | 37.7 | 10.4 | −0.90 | 0.56 | 0.14 | 0.24 | 0.05 |
| 1715 | 1.00 | 32.0 | 10.4 | −1.09 | 0.49 | 0.18 | 0.29 | 0.04 |
| 1745 | 1.00 | 26.3 | 10.6 | −0.59 | 0.37 | 0.17 | 0.24 | 0.22 |
| 1815 | 1.00 | 25.8 | 10.6 | −0.47 | 0.53 | 0.20 | 0.17 | 0.10 |

[a]Here $\bar{\tau}$ is mean cloud optical thickness in $1° \times 1°$ grid box, $\sigma$ is spatial standard deviation of pixel cloud optical thickness in $1° \times 1°$ grid box, and $(\bar{\tau}_{n+1} - \bar{\tau}_{n-1})/\sigma_n$ is centered 1-hour difference in mean optical thickness divided by spatial standard deviation.

the relative importance of each scale changing from one day to another.

## References

Ackerman, T. P., and G. M. Stokes (2003), The Atmospheric Radiation Measurement Program, *Phys. Today*, 56, 38–44.

Albrecht, B. A., C. W. Fairall, D. W. Thomson, A. B. White, J. B. Snider, and W. H. Schubert (1990), Surface-based remote sensing of the observed and the adiabatic liquid water content of stratocumulus clouds, *Geophys. Res. Lett.*, 17, 89–920.

Arakawa, A. (1975), Modeling clouds and cloud processes for use in climate models, in *The Physical Basis of Climate and Climate Modeling*, *GARP Publ. Ser.*, vol. 16, pp. 181–197, Int. Counc. for Sci., World Meteorol. Org., Geneva.

Austin, P., Y. Wang, R. Pincus, and V. Kujala (1995), Precipitation in clouds: Observations and modeling results, *J. Atmos. Sci.*, 52, 2329–2352.

Barker, H. W., G. L. Stephens, and Q. Fu (1999), The sensitivity of domain-averaged solar fluxes to assumptions about cloud geometry, *Q. J. R. Meteorol. Soc.*, 125, 2127–2152.

Brenguier, J. L., P. Y. Chuang, Y. Fouquart, D. W. Johnson, F. Parol, H. Pawlowska, J. Pelon, L. Schuller, F. Schroder, and J. Snider (2000), An overview of the ACE-2 Cloudy-Column closure experiment, *Tellus, Ser. B*, 52, 815–827.

Bretherton, C. S., T. Uttal, C. W. Fairwall, S. E. Yuter, R. A. Weller, D. Baumgardner, K. Comstock, R. Wood, and G. B. Raga (2004), The EPIC 2001 stratocumulus study, *Bull. Am. Meteorol. Soc.*, 85, 967–977.

Cahalan, R. F., W. Ridgway, W. J. Wiscombe, T. L. Bell, and J. B. Snider (1994), The albedo of fractal stratocumulus clouds, *J. Atmos. Sci.*, 51, 2434–2455.

Charney, J. G. (1979), *Carbon Dioxide and Climates: A Scientific Assessment*, 33 pp., Natl. Acad. Press, Washington, D. C.

Clothiaux, E. E., T. P. Ackerman, G. G. Mace, K. P. Moran, R. T. Marchand, M. A. Miller, and B. E. Martner (2000), Objective determination of cloud heights and radar reflectivities using a combination of active remote sensors at the ARM CART sites, *J. Appl. Meteorol.*, 39, 645–665.

Considine, G., J. A. Curry, and B. Wielicki (1997), Modeling cloud fraction and horizontal variability in marine boundary layer clouds, *J. Geophys. Res.*, 102, 13,517–13,525.

Davis, A., A. Marshak, R. Cahalan, and W. Wiscombe (1997), The Landsat scale break in stratocumulus as a three-dimensional radiative transfer effect: Implications for cloud remote sensing, *J. Atmos. Sci*, 54, 241–260.

Del Genio, A. D., M. S. Yao, W. Kovari, and K. K. W. Lo (1996), A prognostic cloud water parameterization of global climate models, *J. Clim.*, 9, 270–304.

Dong, X., P. Minnis, G. Mace, W. Smith, M. Poellot, R. Marchand, and A. Rapp (2002), Comparisons of stratus cloud properties deduced from surface, GOES, and aircraft data during the March 2000 ARM cloud IOP, *J. Atmos. Sci.*, 23, 3265–3284.

Frisch, A. S., C. W. Fairall, and J. B. Snider (1995), Measurement of stratus cloud and drizzle parameters in ASTEX with a $K_\alpha$-band Doppler radar and a microwave radiometer, *J. Atmos. Sci.*, 52, 2788–2799.

Fu, Q., B. Carlin, and G. Mace (2000), Cirrus horizontal inhomogeneity and OLR bias, *Geophys. Res. Lett.*, 27, 3341–3344.

Gerber, H., B. G. Arends, and A. S. Ackerman (1994), New microphysics sensor for aircraft use, *Atmos. Res.*, 31, 235–252.

Hartmann, D. L. (1993), Radiative effects of clouds on Earth's climate, in *Aerosol-Cloud-Climate Interactions*, edited by P. V. Hobbs, pp. 151–170, Elsevier, New York.

Hogan, R. J., and A. J. Illingworth (2000), Deriving cloud overlap statistics from radar, *J. Geophys. Res.*, 105, 2903–2909.

Intergovernmental Panel on Climate Change (IPCC) (2001), *Climate Change 2001: The Scientific Basis*, edited by J. T. Houghton et al., 881 pp., Cambridge Univ. Press, New York.

Kim, B., S. E. Schwartz, M. A. Miller, and Q. Min (2003), Effective radius of cloud droplets by ground-based remote sensing: Relationship to aerosol, *J. Geophys. Res.*, 108(D23), 4740, doi:10.1029/2003JD003721.

Liljegren, J. C. (2000), Automatic self-calibration of ARM microwave radiometers, in *Microwave Radiometry and Remote Sensing of the Earth's Surface and Atmosphere*, edited by P. Pampaloni and S. Paloscia, pp. 433–441,VSP Press, Utrecht, Netherlands.

Liljegren, J. C., E. E. Clothiaux, G. G. Mace, S. Kato, and X. Dong (2001), A new retrieval for cloud liquid water path using a ground-based microwave radiometer and measurements of cloud temperature, *J. Geophys. Res.*, 106, 14,485–14,500.

Lohmann, U., and E. Roeckner (1996), Design and performance of a new cloud microphysics scheme developed for the ECHAM general circulation model, *Clim. Dyn.*, 12, 557–572.

Mellor, G. L. (1977), Gaussian cloud model relations, *J. Atmos. Sci.*, 34, 356–358.

Miller, M. A., M. P. Jenson, and E. E. Clothiaux (1998), Diurnal cloud and thermodynamic variations in the stratocumulus transition regime: A case study using in situ and remote sensors, *J. Atmos. Sci.*, 55, 2294–2310.

Minnis, P., W. L. Smith, D. F. Young, L. Nguyen, A. D. Rapp, P. W. Heck, and M. M. Khaiyer (2002), Near-real-time retrieval of cloud properties over the ARM CART Area from GOES data, paper presented at Twelfth Atmospheric Radiation Measurement Science Team Meeting, U. S. Dept. of Energy, St. Petersburg, Fla.

Nicholls, S., and J. Leighton (1986), An observational study of the structure of stratiform cloud sheets: I. Structure, *Q. J. R. Meteorol. Soc.*, *112*, 431–460.

Pincus, R., S. A. McFarlane, and S. A. Klein (1999), Albedo bias and the horizontal variability of clouds in subtropical marine boundary layers: Observations from ships and satellites, *J. Geophys. Res.*, *104*, 6183–6191.

Pincus, R., H. W. Barker, and J. Morcrette (2003), A fast, flexible, approximate technique for computing radiative transfer in inhomogeneous cloud fields, *J. Geophys. Res.*, *108*(D13), 4376, doi:10.1029/2002JD003322.

Pomroy, H. R., and A. J. Illingworth (2000), Ice cloud inhomogeneity: Quantifying base in emissivity from radar observations, *Geophys. Res. Lett.*, *27*, 2101–2104.

Sassen, K., G. G. Mace, Z. Wang, M. R. Poellot, S. M. Sekelsky, and R. E. McIntosh (1999), Continental stratus clouds: A case study using coordinated remote sensing and aircraft measurements, *J. Atmos. Sci.*, *56*, 2345–2358.

Sellers, W. D. (1976), A two-dimensional global climate model, *Mon. Weather Rev.*, *104*, 233–248.

Slingo, J. M. (1980), A cloud parameterization scheme derived from GATE data for use with a numerical model, *Q. J. R. Meteorol. Soc.*, *106*, 747–770.

Slingo, A., S. Nicholls, and J. Schmetz (1982), Aircraft observation of marine stratocumulus during JASIN, *Q. J. R. Meteorol. Soc.*, *108*, 833–856.

Smith, S. A., and A. D. Del Genio (2001), Analysis of aircraft, radiosonde and radar observations in cirrus clouds observed during FIRE-II: The interactions between environmental structure, turbulence, and cloud microphysical properties, *J. Atmos. Sci.*, *58*, 451–461.

Smith, S. A., and A. D. Del Genio (2002), A simple conceptual model of cirrus horizontal inhomogeneity and cloud fraction, *Q. J. R. Meteorol. Soc.*, *128*, 149–171.

Sommeria, G., and J. W. Deardorff (1977), Subgrid-scale condensation in models of nonprecipitating clouds, *J. Atmos. Sci.*, *34*, 344–355.

Sundqvist, H. (1978), A parameterization scheme for non-convective condensation including prediction of cloud water content, *Q. J. R. Meteorol. Soc.*, *104*, 677–690.

Tiedtke, M. (1996), An extension of cloud-radiation parameterization in the ECMWF model: The representation of subgrid-size variation of optical depth, *Mon. Weather Rev.*, *124*, 745–750.

Tompkins, A. M. (2002), A prognostic parameterization for the subgrid-scale variability of water vapor and clouds in large-scale models and its use to diagnose cloud cover, *J. Atmos. Sci.*, *59*, 1917–1942.

Wielicki, B. A., and L. Parker (1994), Frequency distributions of cloud liquid water path in oceanic boundary layer cloud as a function of regional cloud fraction, in *Proceedings of the Eighth Conference on Atmospheric Radiation*, pp. 415–417, Am. Meteorol. Soc., Boston, Mass.

Wood, R., and J. Taylor (2001), Liquid water path variability in unbroken marine stratocumulus cloud, *Q. J. R. Meteorol. Soc.*, *127*, 2635–2662.

Zhu, P., B. Albrecht, and J. Cottschalck (2001), Formation and development of nocturnal boundary layer clouds over the Southern Great Plains, *J. Atmos. Sci.*, *58*, 1409–1426.

------------------

B.-G. Kim, Department of Atmospheric Environmental Sciences, Kangnung National University, 123 Jibyeondong, Gangnung, Gangwondo 210-702, Korea. (bgk@kangnung.ac.kr)

S. A. Klein, Atmospheric Science Division, Lawrence Livermore National Laboratory, P.O. Box 808, Livermore, CA 94551, USA.

J. R. Norris, Scripps Institution of Oceanography, University of California, San Diego, La Jolla, CA 92037, USA.
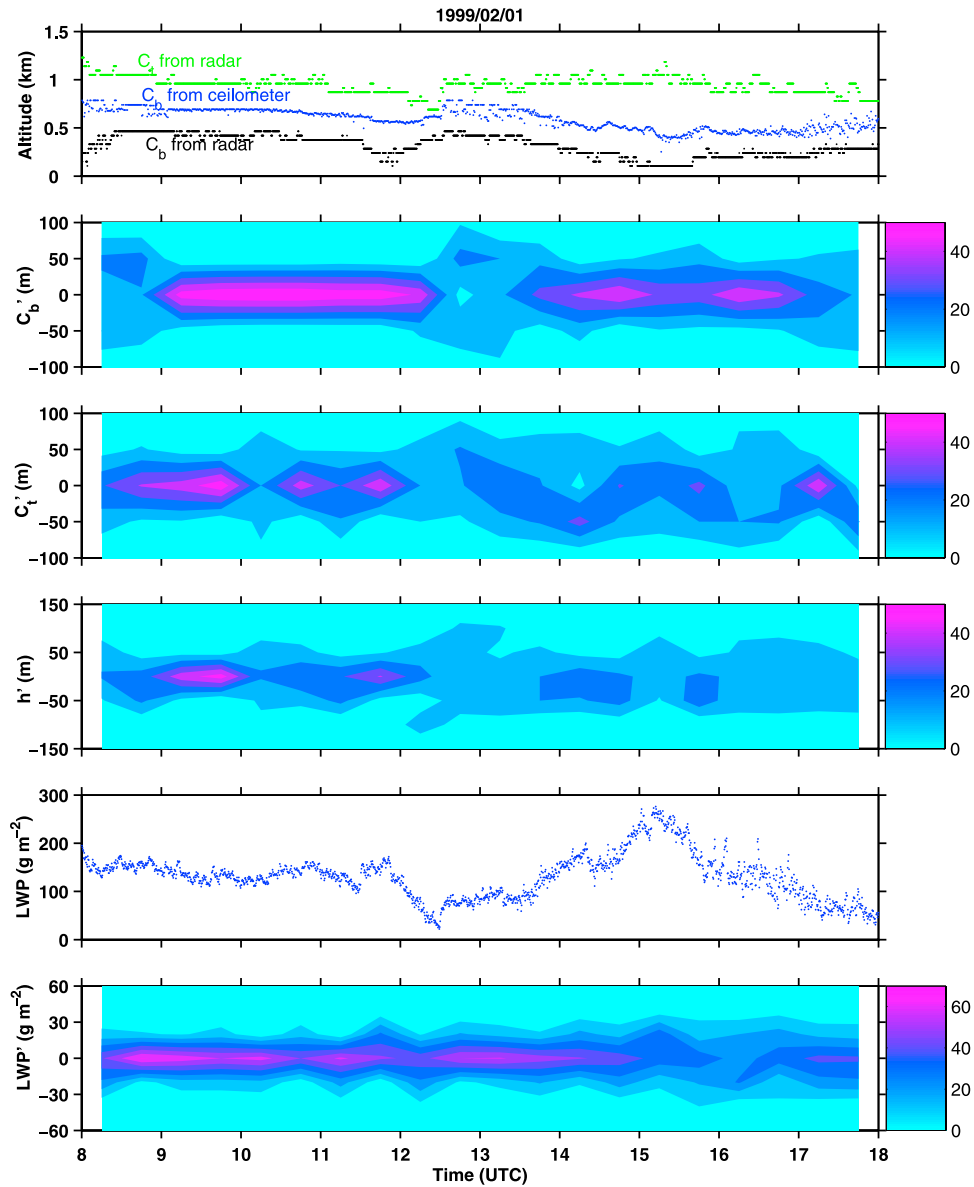
**Figure 1.** Time series of cloud boundaries (base height $C_b$, top height $C_t$), cloud thickness $h$, and LWP on 1 February 1999, also with PDFs of their anomalies ($C'_b$, $C'_t$, $h'$, and LWP$'$). For each 30-min. interval the PDF of anomalies is shown along the vertical axis and the PDFs for various times are shown one after another along the horizontal axis.
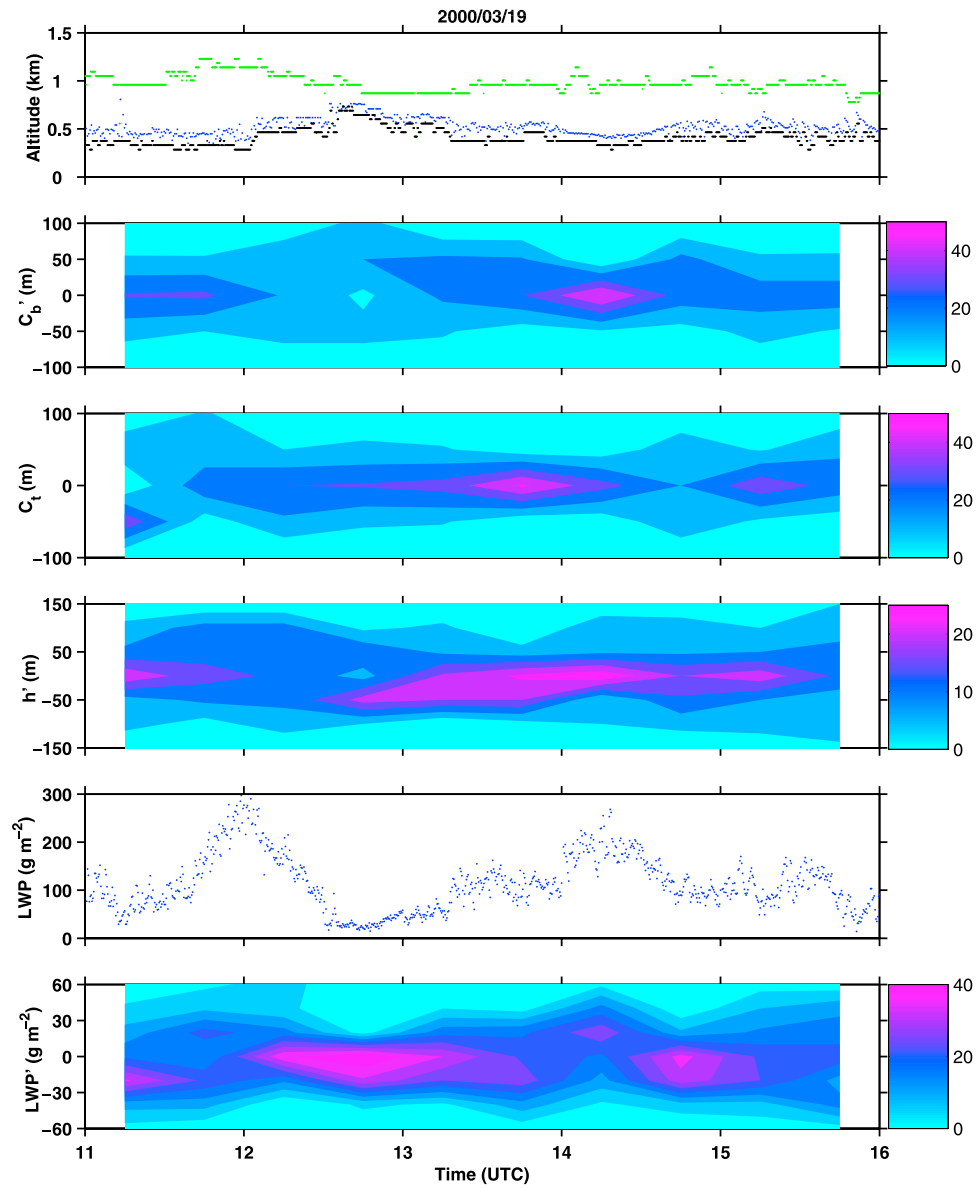
KIM ET AL.: LIQUID WATER CLOUD VARIABILITY



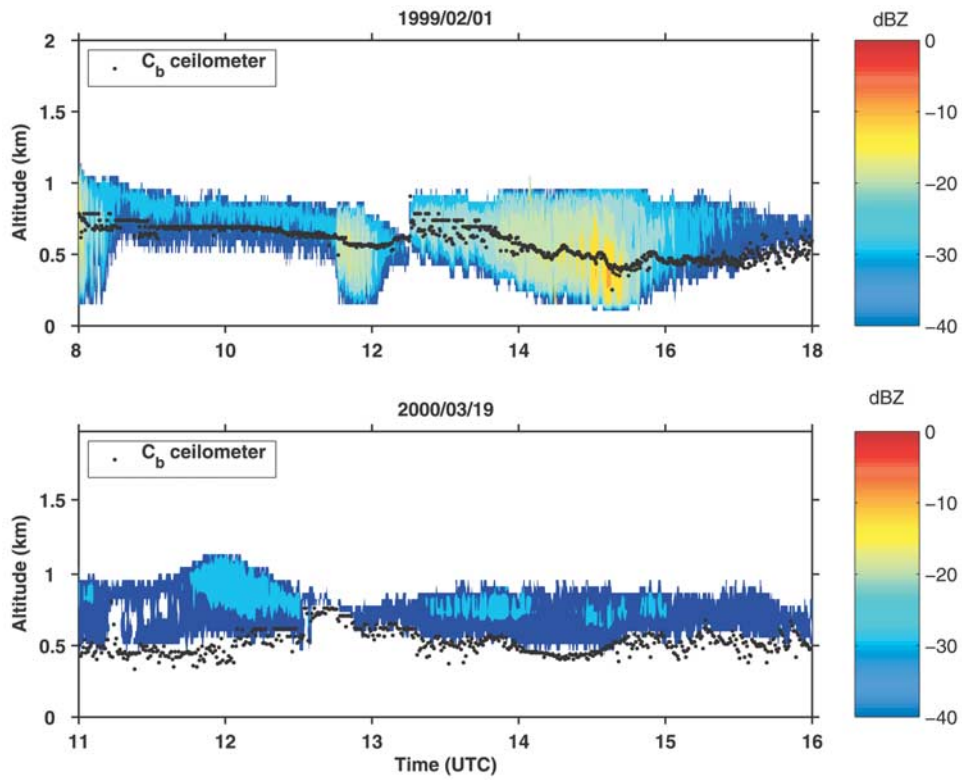**Figure 2.** The same as in Figure 1 but for 19 March 2000.

**Figure 4.** Time-height plot of MMCR reflectivity (dBZ from −40 to 0) at SGP on 1 February 1999 and 19 March 2000. Black dots indicate the cloud base from the ceilometer.
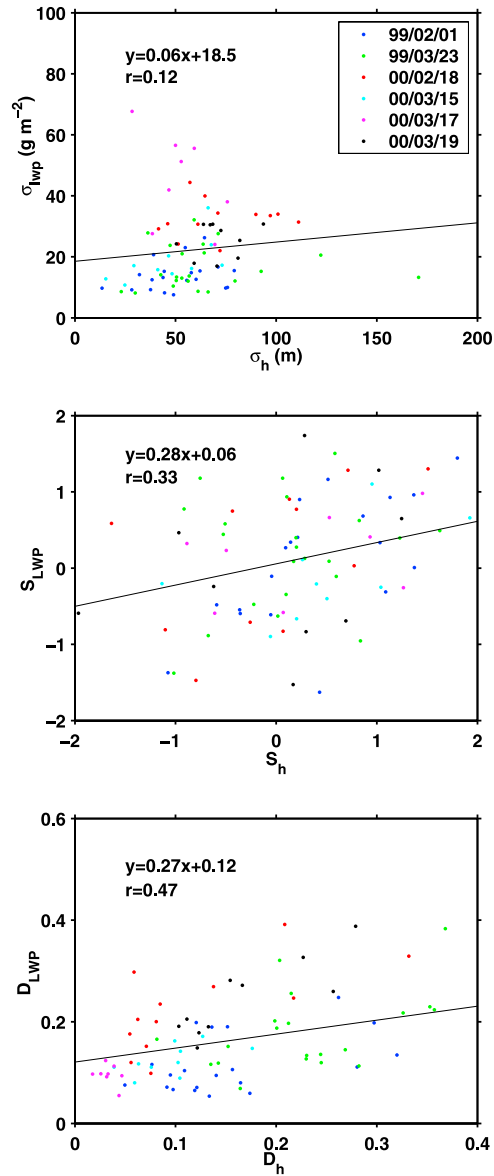
**Figure 8.** Scatterplots of standard deviation $\sigma$, skewness $S$, and dispersion $D$ of the detrended LWP versus those of detrended cloud thickness for 30-min intervals. Solid line denotes the regression line for both variables. These plots are limited to six cases with ceilometer data.